STEADY STATE PRIMARY FREQUENCY ESTIMATION FOR MICROGRID TRANSFERRING MODE USING DISTRIBUTED SLACK BUS LOAD FLOW ANALYSIS

NITHIWAT INTHARASOMCHAI

A Thesis Submitted in Partial Fulfillment of the Requirements for the

Degree of Master Engineering in Electrical Engineering

Suranaree University of Technology

Academic Year 2020

การประเมินความถี่ปฐมภูมิแบบคงตัวสำหรับไมโครกริดที่กำลังถ่ายโอนสถานะ
โดยใช้การวิเคราะห์การไหลของกำลังงานไฟฟ้าแบบกระจายบัสสแลค

นายนิทิวัฒน์ อินทรสมใจ

วิทยานิพนธ์นี้เป็นส่วนหนึ่งของการศึกษาตามหลักสูตรปริญญาวิศวกรรมศาสตรมหาบัณฑิต
สาขาวิชาวิศวกรรมไฟฟ้า
มหาวิทยาลัยเทคโนโลยีสุรนารี
ปีการศึกษา 2563

STEADY STATE PRIMARY FREQUENCY ESTIMATION FOR MICROGRID TRANSFERRING MODE USING DISTRIBUTED SLACK BUS LOAD FLOW ANALYSIS

Suranaree University of Technology has approved this thesis submitted in partial fulfillment of the requirements for a Master's Degree.

Thesis Examining Committee

(Assoc. Prof. Dr. Nit Petcharaks)
Chairperson

(Assoc. Prof. Dr. Keerati Chayakulkheeree)
Member (Thesis Advisor)

(Assoc. Prof. Dr. Thanatchai Kulworawanichpong)
Member

(Asst. Prof. Dr. Uthen Leeton)
Member

(Assoc. Prof. Dr. Chatchai Jothityangkoon)
Vice Rector for Academic Affairs
and Quality Assurance

(Assoc. Prof. Dr. Pornsiri Jongkol)
Dean of Institute of Engineering

นิทิวัฒน์ อินทรสมใจ : การประเมินความถี่ปฐมภูมิแบบคงตัวสำหรับไมโครกริดที่กำลังถ่ายโอนสถานะโดยใช้การวิเคราะห์การไหลของกำลังงานไฟฟ้าแบบกระจายบัสสแลค (STEADY STATE PRIMARY FREQUENCY ESTIMATION FOR MICROGRID TRANSFERRING MODE USING DISTRIBUTED SLACK BUS LOAD FLOW ANALYSIS)
อาจารย์ที่ปรึกษา : รองศาสตราจารย์ ดร.กีรติ ชยะกุลคีรี, 70 หน้า

คำสำคัญ : การถ่ายโอนสถานะของไมโครกริด/การไหลของกำลังไฟฟ้า/ส่วนเบี่ยงเบนความถี่

วิทยานิพนธ์เล่มนี้ได้เสนอวิธีการตรวจสอบและแนวทางในการปรับปรุงส่วนเบี่ยงเบนความถี่ของระบบไมโครกริดภายขณะที่ไมโครกริดอยู่ในช่วยการถ่ายโอนโหมดการทำงาน โดยใช้การควบคุมของแบบจำลองเครื่องกำเนิดไฟฟ้าเสมือนในการปรับปรุงส่วนเบี่ยงเบนความถี่ ผลการวิจัยพบว่าการวิเคราะห์การไหลของกำลังไฟฟ้าแบบกระจายบัสสแลคที่ถูกนำเสนอสามารถนำมาใช้ในการวิเคราะห์หาส่วนเบี่ยงเบนความถี่ของไมโครกริดในช่วงขณะที่ถ่ายโอนโหมดได้ นอกจากนี้แบบจำลองเครื่องกำเนิดไฟฟ้าเสมือน ยังสามารถใช้เพื่อเพิ่มประสิทธิภาพในการควบคุมเบี่ยงเบนความถี่ของไมโครกริดได้ ในวิทยานิพนธ์นี้วิธีการดังกล่าวถูกนำเสนอภายใต้การคำนวณการไหลของกำลังไฟฟ้าตามแบบของนิวตัน-ราฟสัน ซึ่งถูกแก้ไขเพื่อให้สามารถหาส่วนเบี่ยงเบนความถี่ในระบบได้ และในขณะเดียวกันก็ใช้เทคนิคสมการการแกว่งควบคู่ไปด้วยเพื่อสามารถเปรียบเทียบและพิสูจน์ความแม่นยำของวิธีการที่ได้นำเสนอไป

สาขาวิชา วิศวกรรมไฟฟ้า
ปีการศึกษา 2563

ลายมือชื่อนักศึกษา นิทิวัฒน์ อินทรสมใจ
ลายมือชื่ออาจารย์ที่ปรึกษา

NITHIWAT INTHARASOMCHAI : STEADY STATE PRIMARY FREQUENCY ESTIMATION FOR MICROGRID TRANSFERRING MODE USING DISTRIBUTED SLACK BUS LOAD FLOW ANALYSIS. THESIS ADVISOR : ASSOC. PROF. KEERATI CHAYAKULKHEEREE, Ph.D. 70 PP.

Keyword : Microgrid transferring mode/Frequency deviation/Load flow

This thesis proposes the method to investigate and improve the frequency deviation of microgrid system under transferring mode condition using virtual generator droop control model. The results shown that the proposed DSLF can be used to analyze the frequency deviation of microgrid during transferring mode. In addition, the virtual synchronous generator can be used to enhance the frequency deviation of microgrid under transferring mode.

In the proposed method, Newton-Raphson distributed slack bus load flow (DSLF) was modified to incorporating and generation control equations to find the primary frequency deviation. Meanwhile, the swing equation technique was used to prove the accuracy of DSLF.

School of Electrical Engineering | Student's Signature ______

Academic Year 2020 | Advisor's Signature ______

ACKNOWLEDGMENT

This thesis was successfully completed. The author would like to thank those involved in providing academic advice and operational I would like to thank my family for their encouragement throughout the research. Thank you to thesis advisor Assoc. Prof. Dr. Keerati Chayakulkheeree for giving advice and advice. Something that has always been useful to me. Thank you, School of Electrical Engineering, for always taking care of me. Thank you, Suranaree University of Technology, for giving me the opportunity to study here. Finally, I thank myself for not giving up on the problems that arise.

From now on, I intend to study and research to be an important person in the country's development.

Nithiwat Intharasomchai

TABLE OF CONTENTS

Page

TABLE OF CONTENTS (Continued)

Page

LIST OF TABLES

Table Page

LIST OF FIGURES

Figure **Page**

SYMBOLS AND ABBREVIATIONS

$\boldsymbol{D}$	=	damping coefficient
F	=	actual frequency of system
F_0	=	schedule frequency of system
$\boldsymbol{H}$	=	inertia constant
$\boldsymbol{J}$	=	rotor of moment of inertia
$\boldsymbol{M}$	=	angular momentum
NB	=	number of buses
NG	=	number of generator's buses
$\boldsymbol{p}$	=	number of poles on a generator
$\boldsymbol{P_e}$	=	electromagnetic active power
$\boldsymbol{P_i}$	=	real power at bus *i*
$P_{cal,i}$	=	real power flow calculates at bus *i*
$\boldsymbol{P_d}$	=	damping powers
P_{D_i}	=	real power demand at bus *i*
P_{G_i}	=	real power generation at bus *i*
$P_{G_i^o}$	=	schedule of real power generation at bus *i*
P_m	=	mechanical active power
$\boldsymbol{P_{max}}$	=	maximum active power transferred
Q_{G_i}	=	reactive power generation at bus *i*
Q_{D_i}	=	reactive power demand at bus *i*
$Q_{cal,i}$	=	reactive power flow calculates at bus i
r_i	=	speed-droop on turbine governor in generating plant connected to bus i
$\boldsymbol{S_{base}}$	=	system base power
$\boldsymbol{t_s}$	=	setting time
$\boldsymbol{W_k}$	=	kinetic energy of the rotating masses
$\lvert\boldsymbol{E}\rvert$	=	steady state excitation voltage magnitude

SYMBOLS AND ABBREVIATIONS (Continued)

$\|V_i\|$	=	voltage magnitude at bus i
$\|X\|$	=	reactance magnitude of generator bus and infinite bus
$\|Y_{i,k}\|$	=	admittance magnitude of bus i and bus k
$\theta_{i,k}$	=	admittance angle of bus i and bus k
δ_i	=	angle of voltage at bus i
δ_m	=	angular displacement
δ_o	=	power angle before disturbance
ω_m	=	rotor angular velocity
ω_s	=	electric angular velocity
α_i	=	participation factor of generator connected to bus i
ζ	=	dimensionless damping ratio
τ	=	response time constant
ΔF	=	steady-state frequency deviation
ΔG	=	static area control error
ΔP_{G_i}	=	real power generation deviation at bus i
ΔP_i	=	real power deviation at bus i
ΔQ_i	=	reactive power deviation at bus i
$\Delta \delta_i$	=	angle of voltage deviation at bus i
$\Delta \|V_i\|$	=	deviation of voltage magnitude at bus i

CHAPTER 1

INTRODUCTION

1.1 General Introduction

Over the past decade, the generation, transmission, and distribution of electrical power grid systems have been continuously developed to enhance the reliability and stability of the end-users. Microgrid (MG) is the new important key of the system that has been studied and developed. An MG is a local power grid with the ability to stabilize the local system when disconnected from the main power grid (MPG). Moreover, if the MPG needs electric power, MG can even supply the electricity to the MPG. Due to the advantage of the MG concept, many research and developments had been introduced in this area. In Thailand, MG is also included in the master plan to study the impacts and approach to application with Thailand in the future.

1.2 Problem Statement

Thailand has the policy to promote energy security and efficiency according to the Energy Master Plan 2015-2035. The objectives of the Energy Master Plan include two main objectives: energy security, and Environment-friendly society. The objectives of the Energy Security Master Plan consist of various elements, including reliability in the supply of energy to meet demand with economic consideration. Distribution of energy sources and types to reduce risks from various factors is also under consideration including energy efficiency management, which will help reduce the burden of energy supply. The master plan also concerns develop knowledge and technology, along with enhancing national security. Therefore, with the high drama in distributed energy resources, many distribution systems have been shifted to the MG structure.

Generally, the MG operating mode consists of connected and islanded mode. However, as the microgrid transfers the operating mode, there are consequences for frequency and voltage (primary control) and effect on power changes (secondary control). Most of these effects were analyzed using the transfer function method which is very complicated to analyze with large systems. Over the past decade, many MG related research has been presented. The structure of the MG, which has been described as an MG is a cluster of distributed generations (DGs), energy storage system (ESS), and loads within clearly determine electrical boundaries, which acts as a single controllable entity with respect to the grid, as determine by the MG Exchange Group, an ad hoc group of experts and implementers of MG technology. The operating condition of MG can be divided into different modes as shown in Fig 1.1.

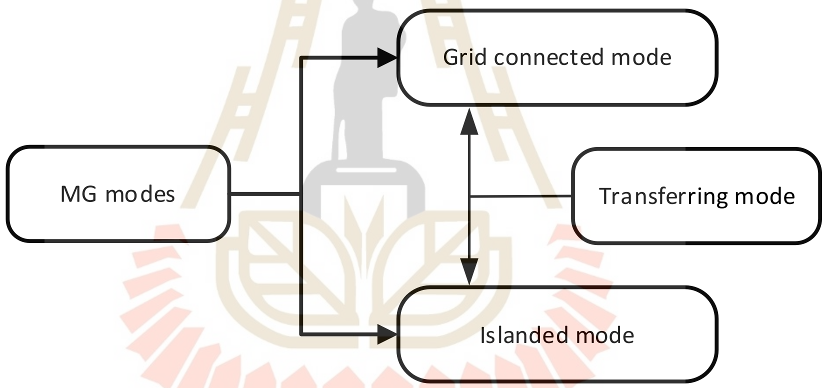

Figure 1.1 Operation modes of MG

Therefore, this thesis aimed at proposing the methodology for investigating the MG frequency deviation using steady state analysis model. The proposed method is expected to be a benefit in avoiding transfer function parameters determination, especially for large scale MG.

1.3 Research objectives

The objectives of this research are as follow,

1) To be able to find the frequency deviation using the Newton-Raphson load flow method.

2) To compare DSLF method to Swing equation considering speed droop.

3) To mitigate the large frequency deviation problem using virtual generator speed droop is controlled by energy storage system.

1.4 Scope and limitations

In this thesis, DSLF is used for determining the steady state frequency deviation from MG transferring mode. DSLF was proposed to test with two systems as follows:

1) the modified IEEE radial distribution 33-bus test system,

2) the modified IEEE radial distribution 69-bus test system.

Moreover, investigation and reduction steady state frequency deviation was proposed in this thesis. In the proposed method for reduction steady state frequency deviation using virtual generator droop control by energy storage system.

1.5 Conception

Usually, the frequency deviation is determined by using transfer functions which are difficult to obtain the correct parameters under difference condition. Therefore, this thesis proposes a method to determine steady state frequency deviation for frequency deviation of MG in transferring mode. The virtual generation by energy storage system is increased in test system models consequently can be control the speed droop generation resulting mitigate the frequency deviation

1.6 Research Benefits

The proposed method was able to control the steady state frequency deviation arising from MG mode transfer, useful for operation planning. The frequency deviation problem mitigation using virtual generator droop control by energy storage system in case of unplanned MG disconnecting mode is also investigated.

CHAPTER 2
LITERATURE REVIEW

2.1 Introduction

In this chapter it is responsible for the collection of theories needed to study and related research in the thesis This chapter consists of three topics: load flow, virtual generator, and microgrid and management.

2.2 Load flow

The flow of electrical energy in any electrical system between connected buses is called load flow. Load flow studies are essential for electrical power systems under operating conditions, improvements, and future expansion. Load flow analysis is presented in a variety of formats. In this thesis, analysis is presented in the form distributed slack bus load flow (DSLF).

The process of obtaining normal load flow results differs from that of DSLF, where normal load flow considers only one swing bus, causing the static area control error to be updated only the active power deviation of the generator on the swing bus on a single bus, as $\Delta P_{G,Swing} = \Delta G.$

In contrast, the DSLF load flow calculation process considers every bus as a swing bus, where the static area control errors are averaged according to the participation factor in every active power deviation of the generator, as $\Delta P_{G_i} = \alpha_i \Delta G.$

In practice, locational marginal prices are usually calculated by assembling their three components as the reference prices, the congestion prices, and the loss prices. Explicit formulas for calculating the three components based on the single-slack power-flow formulation can be found in the literature. Wu (2005) presented the formulas for calculating the three components based on a distributed slack bus load flow formulation.

In the enhancement, Chayakulkheeree (2007) proposed method for assessing the proper scheduling of actual power generation in a power system consisting of regulated and deregulated subsystems. A new approach has been developed using a distributed slack bus model. Reducing fuel costs is an objective function for each generator subsystem participating in economic delivery in a deregulated market. Kabir et al. (2014) reported the development of a slack bus integration method in Jacobians for Studying the NR load flow, this method involves constructing a loss equation, and then formulating a condition for the condition to be incorporated into the elements of the Jacobian matrix. Ping Yan (2001) presented a methodology for evaluating optimization of fuel cost for active power of generator in power system using distributed slack bus load flow base on participation factor.

DSLF can be applied to a variety of purposes and is commonly used to simulate a competitive power market. The advantage of DSPF is its ability to compute the frequency deviation when the ACE is treated as fixed value. For this reason, DSLF is a suitable tool for this thesis. To determine the frequency deviation occurring in the system. A comparison of the relevant researches are shown in Table 2.1.

Table 2.1 Summary of DSLF literatures

Proposed	Method	Objective	Model system	Significant finding
Yan, 2001.	DSLF	Presents the formulas for calculating the components • The reference prices • The congestion prices • The loss price	Modified IEEE 30-Bus system	DSLF is worked to calculating the three components.
Chayakulkheeree, 2007.	DSLF	Minimize fuel cost in the economic dispatch in deregulated market. • OPF	Modified IEEE 30-Bus system	26.6 percent cost reduction
Kabir et al, 2014.	DSLF	Using distributed slack bus load flow method considering slack bus into the Jacobians for N-R load flow study.	• 6-Bus system • IEEE 30-Bus system • IEEE 57-Bus system	The new technique is also applied to a case of loss distributed among different generator buses.
Wu et al, 2005.	DSLF	This letter presents the formulas for the LMP decomposition using a distributed-slack power-flow formulation	None	The formulas can be used to calculate the LMPs by assembling their components.

2.3 Analysis of power systems with swing equations

Synchronous generators can inject sufficient energy into the power system to maintain the energy balance in the system. However, inertia in synchronous generators suppresses sudden deviation of frequency and stabilizes. The distributed generator is static and does not have a rotating part to store kinetic energy, and the moment of grid inertia is reduced and significantly affects the stability of the system. Consequently, swing equations are commonly used in power analysis by simulating synchronous generators.

Thomas et al (2018) presented the concept of analysis based on the swing equation of a synchronous generator. Leng and Polmai (2019) proposed for Reduce the lacking the grid-forming ability and inertia of DG. Two case studies have been conducted, such as power sharing and transient loading. The results show that VSG provides better performance compared to the modulated drop control when large load shifts are used. Palacio R. et al (2017) used VSG based controller with active and reactive power tracking is shown in fig 2.1.

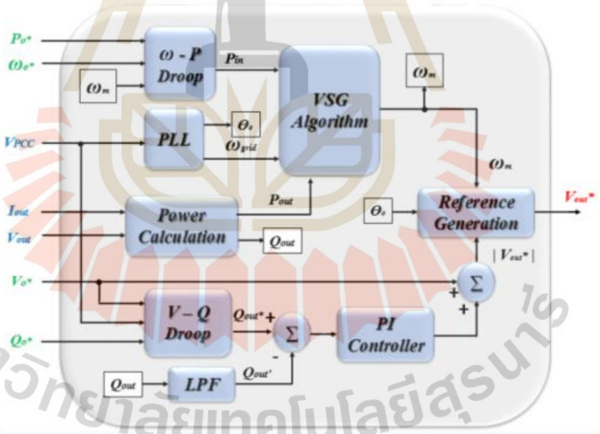

Figure 2.1 VSG based controller with active and reactive power tracking

All measurements are inputs references for this controller. Using droop laws and solving the swing equation.

Zhang et al (2018) have presented a very interesting VSG is applied to the power electronic converters to mimic the rotating mass and damping property of a conventional synchronous generator. The block diagram of the traditional frequency control and the virtual inertia control of the VSG is shown in fig 2.2.

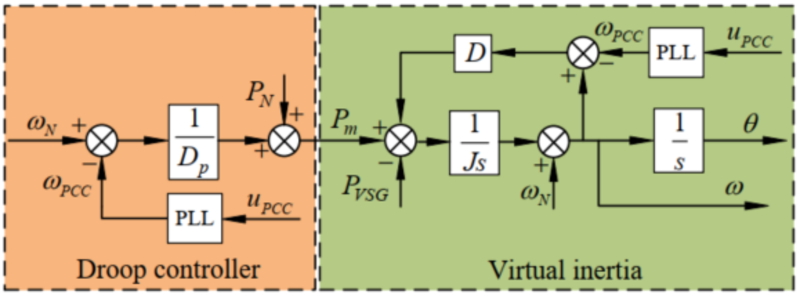

Figure 2.2 Active power controller of VGS

Mansour et al (2016) presented in a different way to control droop by adding Voltage/Frequency inverter system under variable load. Droop based control system for the VF inverter as shown in fig 2.3.

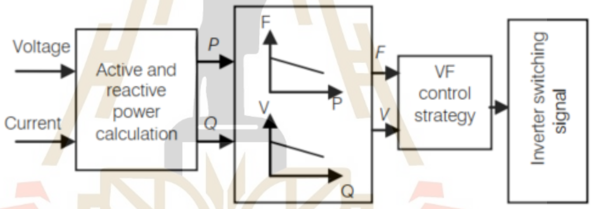

Figure 2.3 Droop based control system for the VF inverter

Many control schemes were applied to the inverter to allow the inverter to act like a VSG. The VSG design included reduction characteristics, swing equations, and synchronous generators damping properties. Some of the studies involving speed droop control are compared in Table 2.2.

Table 2.2 Analysis of power systems with swing equations

Proposed	Strategy	Objective	Significant finding
Thomas et al, 2018.	• VSG	Analyzes the equivalency between the VSG and droop control in MGs.	Also, a simplified stability analysis based on the swing equation of a synchronous generator or VSG can be applied to the p-ω droop controllers.
Leng et al, 2019.	• Modified droop control • VSG	Investigate the performance of modified droop control with VSG control.	Both methods have the same accuracy for power-sharing. While there is load transition, the VSG has a better performance with small frequency deviation compare to modified droop control.
Mansour et al, 2016.	• Droop based Control	One DG unit is controlled to set the voltage and frequency of the MG.	MG system transition from grid-connected to islanded mode without the need to wait for the islanding detection signal.
Palacio R. et al, 2017.	• VSG	This paper presents a virtual synchronous generator (VSG) based topology for microgrids applications.	Resulting confirm a similar behavior with synchronous generators.

Table 2.2 Analysis of power systems with swing equations (Continued)

Proposed	Strategy	Objective	Significant finding
Zhang et al, 2018.	• VSG	Accurate small-signal model of a multiple parallel VSG system was established	The decoupling of the active power and reactive power was realized well. It implies that the enhanced VSG control can track the load transition rapidly and accurately without oscillation.
Nogami et al, 2018.	• VSG model-based control PV	Improve the stability of the power system	The simulation results show that the proposed control is more effective for the system stability improvement than the constant power control of the PV.
Yue Hao and Hua Li, 2019.	• VSG	to solve the low inertia problem and damping effect brought by the large-scale integration of Distributed Generators (DGs) into the grid.	the proposed method can effectively improve the safety and stability and has good practicability.
Vikash et al, 2020.	• VSG	for supporting the system stability by giving the similar characteristics of the SG.	The VSG incorporates the swing equation of the traditional SG to include the property of virtual inertia, using which the rate of change of frequency of the system is reduced.

2.4 Microgrid (MG)

In common practice an MG can operate while connected to a MV network. When a preplanned or unplanned event like holding or occurring fault occurs in the MV network it is possible to cause the islanding state in the MG. In this Paper the operation of the MV network in the islanding mode and how to control the MG by using the controlling structure are investigated. In this paper the conventional droop method has been described and a new controlling method for controlling the MG are also proposed which in the first method the AC power theory for the controlling of the MG. For comparing these two methods with the controlling method, which is proposed in reference, these three methods have been simulated with PSCAD/EMTDC software. (Yasser R. K. and Mohammad H. K., 2018).

In the recent years, there has been a growing interest in the concept of MGs to integrate distributed generation systems and to provide higher reliability for critical loads. Several MG demonstrations projects have been implemented to investigate further and advance this emerging concept. This article provides a detailed review of MG systems. It describes different architectures, including AC, DC, and hybrid systems. Various MG components, including sources, converters, and loads, are illustrated. MG management and controls are discussed, and a modified natural droop control is described in detail. Both physical layers and standard protocols are explained for communication in the MG structure. The unique protection complexities have been raised and discussed in the presence of distributed generations and bidirectional power flow. A demonstration of a military MG system at Fort Sill is illustrated, and the experiment of a typical MG operation scenario is provided. (Qiang F., Adel N., Ashishkumar S., Abedalsalam B. A., Luke W., and Vijay B., 2015).

Renewable resources can be used for the energy scarcity facing now. For the optimum usage of renewable resources, system called MG. It can be operated in two modes. In the normal condition the MG is connected to the utility grid. Current control is given during this mode to give preset power. In this mode, when there is any fault or maintenance in the main grid the MG is islanded either to prevent spreading of fault to the MG or to prevent accidents. When the intentional islanding is done, the control is given to maintain the voltage. Thus, constant control is given to the loads during this mode. Depending on the generation of MG side the intelligent load shedding is implemented. The critical loads are maintained without any power quality issues. Simulation is performed using MATLAB \ Simulink software. Simulation of controls during different modes, islanding detection algorithm and intelligent load shedding is given here (Megha Prakash.M. and Jasmy P., 2016).

Droop control is often used for smooth switching of MG. In this paper, a new robust droop control strategy is proposed by designing a compensatory sliding mode controller to enhance the system stability. The load angle-voltage is used for droop control variable, and state space equations are established based on the droop control structure. In addition, a compensatory nonlinear controller is designed via sliding mode control method to mitigate the frequency chattering phenomenon caused by switching of MG operation states, so that system stability and response rapidity are guaranteed. In the end, the simulation results obtained from Matlab/Simulink platform show the validity of the proposed scheme (M. Yang, X. Hongliang, B. Chunyan, W. Shengyi, Z. Han, J. Yuanwei, 2016)

MG has two operating modes, that is the state of being integrated in external grid and the state of island operation and can switch freely between the two states. the method to improve the en\ergy storage model is proposed, and its improved results are validated by simulation experiments, the results show that the new improved storage model is more consistent with theoretical expectations and realities than the original model. (Z. Xiaobo and Z. Baohui, 2014)

Table 2.3 Summary of MG literatures.

Proposed	Topic	Objective	Significant finding
RahmatiKukandeh et al, 2018.	MG Control In Islanding And Connected Mode	this paper regards the evaluation, through numerical simulation, of the inverter-fed MG behavior under islanded operation and connected operation for different load conditions and using different control strategies with limiter for power.	In this paper we have investigate and simulated some approaches for controlling MG as follows: • A full description of the Droop controlling method • Applying the AC power theory as a new approach to control • Simulating the Droop controlling method and two new controlling methods and comparing them
Qiang Fu et al, 2015.	Architectures, Controls, Protection, and Demonstration	This paper provides a detailed review of MG systems. It describes different architectures, including AC, DC, and hybrid systems	The operating nature of MGs is much different from conventional distribution systems for several reasons, including high penetration of DGs, renewable sources, power electronics-based components, and energy storage.
Megha Prakash.M et al, 2016.	Control of MG for Different Modes of Operation	This article describes the controls in each MG operating mode.	the control schemes are capable of maintaining the voltages and currents among permissible levels throughout grid connected and islanding operation modes.

Table 2.3 Summary of MG literatures (Continued)

Proposed	Topic	Objective	Significant finding
Megha Prakash.M et al, 2016.	Control of MG for Different Modes of Operation	This article describes the controls in each MG operating mode.	The control schemes are capable of maintaining the voltages and currents among permissible levels throughout grid connected and islanding operation modes.
MI Yang et al, 2016.	Study on Smooth Switching of MG Operation States Using Sliding Mode Control	Design nonlinear compensation controller, and the compensation signal is attached to the voltage signal generated by the voltage control.	In this paper, angle-voltage droop control is adopted, and a compensatory controller is designed using SMC algorithm. Through the validation of simulating, the stability of system is improved, and smooth switching is achieved by the proposed scheme.
Xiaobo et al, 2019.	Improved MG energy storage device model in MG mode switching process	The method to improve the energy storage model is proposed, and its improved results are validated by simulation experiments.	Both methods have the same accuracy for power-sharing. While there is load transition, the VSG has a better performance with small frequency deviation compared to modified droop control.

CHAPTER 3
METHODOLOGY

3.1 Introduction

In this section presented, the method related to finding the frequency deviation calculated from the load flow was presented in 3.2 and 3.3 presented the theory of VSG simulation that aim to mitigate the effect on the system frequency when the microgrid is operating mode transfer.

3.2 DSLF for MG Frequency Deviation Analysis

In this thesis, the Newton-Raphson Power Flow (NRPF) technique (T. Wu et al, 2005, Yan, 2001 and Chayakulkheeree, 2007) was used to incorporating generation frequency control characteristic. Bus power injections including active and reactive power for every bus can be expressed as,

$$\Delta P_i = (P_{G_i} - P_{D_i}) - P_{cal,i} \ , \ i = 1, \ldots, NB, \tag{3.2.1}$$

$$\Delta Q_i = (Q_{G_i} - Q_{D_i}) - Q_{cal,i} \ , \ i = 1, \ldots, NB, \tag{3.2.2}$$

$$P_{cal,i} = \sum_{k=1}^{NB} |V_i||V_k||Y_{i,k}| \cos\left(\theta_{i,k} + \delta_k - \delta_i\right) \ , \ i = 1, \ldots, NB, \tag{3.2.3}$$

$$Q_{cal,i} = -\sum_{k=1}^{NB} |V_i||V_k||Y_{i,k}| \sin\left(\theta_{i,k} + \delta_k - \delta_i\right) \ , \ i = 1, \ldots, NB. \tag{3.2.4}$$

From the above equation can be formatted in to the Jacobian matrix can be expressed as,

$$\begin{bmatrix} \Delta P_1 \\ \Delta P_2 \\ \vdots \\ \Delta P_{NB} \\ \Delta Q_1 \\ \Delta Q_2 \\ \vdots \\ \Delta Q_{NB} \end{bmatrix} = \begin{bmatrix} \frac{\partial P_1}{\partial \delta_1} & \frac{\partial P_1}{\partial \delta_2} & \cdots & \frac{\partial P_1}{\partial \delta_{NB}} & \frac{\partial P_1}{\partial |V_1|} & \frac{\partial P_1}{\partial |V_2|} & \cdots & \frac{\partial P_1}{\partial |V_{NB}|} \\ \frac{\partial P_2}{\partial \delta_1} & \frac{\partial P_2}{\partial \delta_2} & \cdots & \frac{\partial P_2}{\partial \delta_{NB}} & \frac{\partial P_2}{\partial |V_1|} & \frac{\partial P_2}{\partial |V_2|} & \cdots & \frac{\partial P_2}{\partial |V_{NB}|} \\ \vdots & \vdots & \ddots & \vdots & \vdots & \vdots & \ddots & \vdots \\ \frac{\partial P_{NB}}{\partial \delta_1} & \frac{\partial P_{NB}}{\partial \delta_2} & \cdots & \frac{\partial P_{NB}}{\partial \delta_{NB}} & \frac{\partial P_{NB}}{\partial |V_1|} & \frac{\partial P_{NB}}{\partial |V_2|} & \cdots & \frac{\partial P_{NB}}{\partial |V_{NB}|} \\ \frac{\partial Q_1}{\partial \delta_1} & \frac{\partial Q_1}{\partial \delta_2} & \cdots & \frac{\partial Q_1}{\partial \delta_{NB}} & \frac{\partial Q_1}{\partial |V_1|} & \frac{\partial Q_1}{\partial |V_2|} & \cdots & \frac{\partial Q_1}{\partial |V_{NB}|} \\ \frac{\partial Q_2}{\partial \delta_1} & \frac{\partial Q_2}{\partial \delta_2} & \cdots & \frac{\partial Q_2}{\partial \delta_{NB}} & \frac{\partial Q_2}{\partial |V_1|} & \frac{\partial Q_2}{\partial |V_2|} & \cdots & \frac{\partial Q_2}{\partial |V_{NB}|} \\ \vdots & \vdots & \ddots & \vdots & \vdots & \vdots & \ddots & \vdots \\ \frac{\partial Q_{NB}}{\partial \delta_1} & \frac{\partial Q_{NB}}{\partial \delta_2} & \cdots & \frac{\partial Q_{NB}}{\partial \delta_{NB}} & \frac{\partial Q_{NB}}{\partial |V_1|} & \frac{\partial Q_{NB}}{\partial |V_2|} & \cdots & \frac{\partial Q_{NB}}{\partial |V_{NB}|} \end{bmatrix} \begin{bmatrix} \Delta \delta_1 \\ \Delta \delta_2 \\ \vdots \\ \Delta \delta_{NB} \\ \Delta |V_1| \\ \Delta |V_2| \\ \vdots \\ \Delta |V_{NB}| \end{bmatrix} . \qquad (3.2.5)$$

The generator's prime mover responses and AGC action (A. J. Wood, B. F. Wollengerg, G. B. Sheblé (Eds.), 2014) are included as primary and secondary controls. Active power generation at a bus considered as,

$$\sum_{i=1}^{NG} P_{G_i} = \sum_{i=1}^{NG} P_{G_i^o} + \sum_{i=1}^{NG} \Delta P_{G_i} \;, i = 1, \ldots, NB, \qquad (3.2.6)$$

$$\Delta P_{G_i} = -\frac{1}{r_i}\Delta F + \alpha_i \Delta G \;, i = 1, \ldots, NB, \qquad (3.2.7)$$

$$\sum_{i=1}^{NG} \alpha_i = 1.00 \;, i = 1, \ldots, NB, \qquad (3.2.8)$$

$$\Delta F = F - F_0 . \qquad (3.2.9)$$

Assuming bus one as reference for the purpose of frequency deviation calculations of the system, the linearized equations for Newton-Raphson is corrected from Eq. (3.2.5).

Therefore, this concept can be find the ΔF in primary responsewhen there is sudden change of generation or load so, that is also a simpler and more convenient method than using transfer function. The linearized equations for Newton-Raphson is corrected can be expressed as,

$$\begin{bmatrix} \Delta P_1 \\ \Delta P_2 \\ \vdots \\ \Delta P_{NB} \\ \Delta Q_1 \\ \Delta Q_2 \\ \vdots \\ \Delta Q_{NB} \end{bmatrix} = \begin{bmatrix} \frac{\partial \mathrm{P}_1}{\partial F} & \frac{\partial \mathrm{P}_1}{\partial \delta_2} & \cdots & \frac{\partial \mathrm{P}_1}{\partial \delta_{NB}} & \frac{\partial \mathrm{P}_1}{\partial |V_1|} & \frac{\partial \mathrm{P}_1}{\partial |V_2|} & \cdots & \frac{\partial \mathrm{P}_1}{\partial |V_{NB}|} \\ \frac{\partial \mathrm{P}_2}{\partial F} & \frac{\partial \mathrm{P}_2}{\partial \delta_2} & \cdots & \frac{\partial \mathrm{P}_2}{\partial \delta_{NB}} & \frac{\partial \mathrm{P}_2}{\partial |V_1|} & \frac{\partial \mathrm{P}_2}{\partial |V_2|} & \cdots & \frac{\partial \mathrm{P}_2}{\partial |V_{NB}|} \\ \vdots & \vdots & \ddots & \vdots & \vdots & \vdots & \ddots & \vdots \\ \frac{\partial \mathrm{P}_{NB}}{\partial F} & \frac{\partial \mathrm{P}_{NB}}{\partial \delta_2} & \cdots & \frac{\partial \mathrm{P}_{NB}}{\partial \delta_{NB}} & \frac{\partial \mathrm{P}_{NB}}{\partial |V_1|} & \frac{\partial \mathrm{P}_{NB}}{\partial |V_2|} & \cdots & \frac{\partial \mathrm{P}_{NB}}{\partial |V_{NB}|} \\ 0 & \frac{\partial \mathrm{Q}_1}{\partial \delta_2} & \cdots & \frac{\partial \mathrm{Q}_1}{\partial \delta_{NB}} & \frac{\partial \mathrm{Q}_1}{\partial |V_1|} & \frac{\partial \mathrm{Q}_1}{\partial |V_2|} & \cdots & \frac{\partial \mathrm{Q}_1}{\partial |V_{NB}|} \\ 0 & \frac{\partial \mathrm{Q}_2}{\partial \delta_2} & \cdots & \frac{\partial \mathrm{Q}_2}{\partial \delta_{NB}} & \frac{\partial \mathrm{Q}_2}{\partial |V_1|} & \frac{\partial \mathrm{Q}_2}{\partial |V_2|} & \cdots & \frac{\partial \mathrm{Q}_2}{\partial |V_{NB}|} \\ \vdots & \vdots & \ddots & \vdots & \vdots & \vdots & \ddots & \vdots \\ 0 & \frac{\partial \mathrm{Q}_{NB}}{\partial \delta_2} & \cdots & \frac{\partial \mathrm{Q}_{NB}}{\partial \delta_{NB}} & \frac{\partial \mathrm{Q}_{NB}}{\partial |V_1|} & \frac{\partial \mathrm{Q}_{NB}}{\partial |V_2|} & \cdots & \frac{\partial \mathrm{Q}_{NB}}{\partial |V_{NB}|} \end{bmatrix} \begin{bmatrix} \Delta F \\ \Delta \delta_2 \\ \vdots \\ \Delta \delta_{NB} \\ \Delta |V_1| \\ \Delta |V_2| \\ \vdots \\ \Delta |V_{NB}| \end{bmatrix} . \qquad (3.2.10)$$

The Newton Raphson iteration process is repeated until the ΔP_i and ΔQ_i in Eq. (3.2.10) for all buses fall within the specified tolerance range. The sequence of operation of such replication processes is shown in Fig. 3.1.

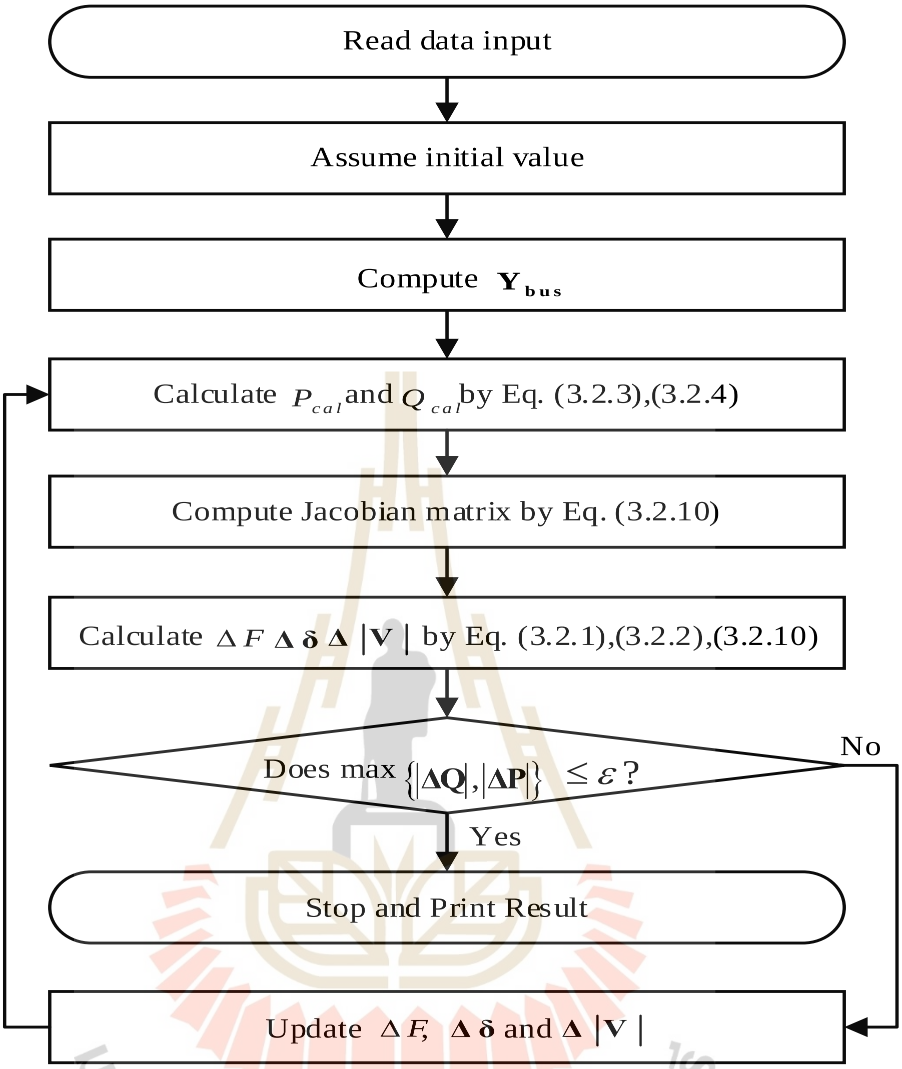

Figure 3.1 Computational procedure of power flow program for finding of the frequency deviation.

3.3 Analysis of power systems with swing equations

A similar study found that most of the studies used swing equations for simulations VSG increase to the MG system to help support the system to be stable.

- VSG Modeling

As there are several VSG control algorithms for the inverter, they can be divided into two types: high-order and low-order models. However, higher order model is more complex than can be realized under the order, so the model has been widely used in recent literature.

The current research is focused on a second-order model of a synchronous generator consisting of mechanical and electrical components. The rotor inertia and damping characteristics of a synchronous generator are reflected by the mechanical rotation equation, known as the oscillation equation.

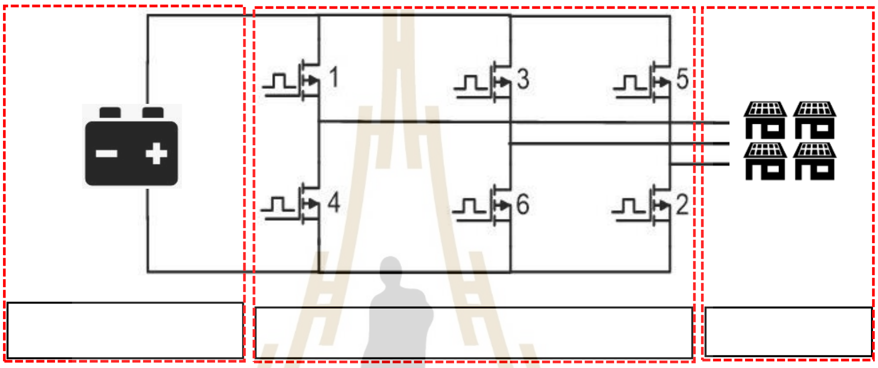

Figure 3.2 Concept of a virtual synchronous generator.

The VSG concept consists of a power source, an inverter and a controller. Shown as Fig 3.2 but the most important thing is Mathematical model in the inverter controller.

- Frequency Response with Swing Equation

Mathematical modeling is an important part of analyzing the operating behavior of power systems. The swing equation is an algorithm for controlling the model according to different situations.

As mentioned at the beginning, the swing equation (Zhang et al, 2018.) can be represented as,

$$J\omega_m \frac{d^2\delta_m}{dt^2} = P_m - P_e, \tag{3.3.1}$$

where Jωm is called the moment of inertia (M),

$$M = J\omega_m, \tag{3.3.2}$$

Swing equation in terms of electrical power angle (δ) is shown as the following equation,

$$\delta = \frac{p}{2}\delta_m, \tag{3.3.3}$$

$$\omega_m = \frac{2}{p}\omega_s, \tag{3.3.4}$$

from Eq. (3.3.2) and Eq. (3.3.3), the swing equation shown in Eq. (3.3.1) shall be changed as follows,

$$\frac{2M}{p}\frac{d^2\delta}{dt^2} = P_m - P_e. \tag{3.3.5}$$

M is related to the kinetic energy of the rotating mass (Wk), using the following equation,

$$M = \frac{2W_k}{\omega_m}, \tag{3.3.6}$$

the swing equation is solved according to the W_k relationship can be expressed as,

$$\frac{2W_k}{\omega_s}\frac{d^2\delta}{dt^2} = P_m - P_e, \tag{3.3.7}$$

The Eq. (3.3.7) when converted to P.U. form is shown as the following equation,

$$\frac{1}{S_{base}}\frac{2W_k}{\omega_s}\frac{d^2\delta}{dt^2}=P_{m,pu.}-P_{e,pu.}, \tag{3.3.8}$$

$$H=\frac{W_k}{S_{base}}. \tag{3.3.9}$$

The inertia constant (*H*) has a characteristic value or a range of values for each class of machines. Table 3.1 shows some typical inertia constants. Inertia constant can be represented as following equation,

Table 3.1 Typical inertia constant of synchronous machine

Type of machine	Inertia constant *H* [MJ/MVA]
Turbine generator:	
Condensing 1800 rpm	9-6
Condensing 3600 rpm	7-4
Noncondensing 3600 rpm	4-3
Waterwheel generator:	
Slow speed < 200 rpm	2-3
High speed > 200 rpm	2-4
Synchronous condenser:	
Large	1.25
Small	1.00
Synchronous motor with load	2.00

For the convenience of using equations to calculate it is important to keep the equation formatting compact.

Electrical power output can be expanded as follows:

$$P_e = \frac{|E'||V|}{|X|}\sin\delta, \tag{3.3.10}$$

$$P_{\max} = \frac{|E'||V|}{|X|}, \tag{3.3.11}$$

from Eq. (3.3.11), the equation of Electrical power output diversifies form as follows,

$$P_e = P_{\max}\sin\delta. \tag{3.3.12}$$

The complete swing equation before the disturbance can be expressed as,

$$\frac{H}{\pi F_0}\frac{d^2\delta}{dt^2} = P_{m,pu.} - P_{\max,pu.}\sin\delta. \tag{3.3.13}$$

But in case the system is disturbed, what will happen to the oscillation equation is that it causes the power angle deviation,

$$\delta = \delta_0 + \Delta\delta. \tag{3.3.14}$$

The impact of disturbances affects the swing equation,

$$\frac{H}{\pi F_0}\frac{d^2\delta_0}{dt^2} + \frac{H}{\pi F_0}\frac{d^2\Delta\delta}{dt^2} = P_{m,pu.} - P_{\max,pu.}(sin\delta_0 cos\Delta\delta + cos\delta_0 sin\Delta\delta) \tag{3.3.15}$$

Since this is a small interference, assuming that $\Delta\delta$ is very small, then

$\cos\Delta\delta \approx 1$ and $\sin\Delta\delta \approx \Delta\delta$

$$\frac{H}{\pi F_0}\frac{d^2\delta_0}{dt^2}+\frac{H}{\pi F_0}\frac{d^2\Delta\delta}{dt^2}=P_{m,pu.}-P_{\max,pu.}sin\delta_0+P_{\max,pu.}cos\delta_0\times\Delta\delta \tag{3.3.16}$$

Compare the pre-disturbance Eq. (3.3.13) swing equation with the post-disturbance Eq. (3.3.16) swing equation to obtain the swing equation in terms of the change in power angle can be expressed as,

$$\frac{H}{\pi F_0}\frac{d^2\Delta\delta}{dt^2}+P_{\max,pu.}\cos\delta_0\times\Delta\delta=0, \tag{3.3.17}$$

$$P_s=P_{\max,pu.}\cos\delta_0, \tag{3.3.18}$$

and designated power variation due to small interference is ΔP

$$\frac{H}{\pi F_0}\frac{d^2\Delta\delta}{dt^2}+P_S\times\Delta\delta=\Delta P. \tag{3.3.19}$$

The swing equation Eq. (3.3.19) is also required in terms of damping power and speed droop. The equation of damping power and speed droop is shown below,

$$P_d=D\frac{d\Delta\delta}{dt}, \tag{3.3.20}$$

$$\Delta P_G=-\frac{1}{2\pi r}\frac{d\Delta\delta}{dt}. \tag{3.3.21}$$

The swing equation with terms of damping power Eq. (3.3.20) and speed droop Eq. (3.3.21) can be represented as follows

$$\frac{d^2\Delta\delta}{dt^2}+(\frac{\pi F_0}{H}D-\frac{F_0}{2Hr})\frac{d\Delta\delta}{dt}+\frac{\pi F_0}{H}P_S\Delta\delta=\frac{\pi F_0}{H}\Delta P. \tag{3.3.22}$$

The natural frequency of oscillation,

$$\omega_n=\sqrt{\frac{\pi F_0}{H}P_s}, \tag{3.3.23}$$

the dimensionless damping ratio,

$$\zeta=\frac{D}{2}\sqrt{\frac{\pi F_0}{HP_s}}. \tag{3.3.24}$$

The result of improving the oscillation equations with ωn and ζ is shown as the following equation,

$$\frac{d^2\Delta\delta}{dt^2}+(2\zeta\omega_n-\frac{F_0}{2Hr})\frac{d\Delta\delta}{dt}+\omega_n^2\Delta\delta=\Delta u, \tag{3.3.25}$$

$$\Delta u=\frac{\pi F_0}{H}\Delta P. \tag{3.3.26}$$

Once the oscillation Eq. (3.3.25) is obtained, the next step is to solve the differential equation problem. From Eq (3.3.25), where $X1 = \Delta\delta$ $X2 = \Delta\omega$

then $\dot{X}1 = X2$ $\dot{X}2 = -(2\zeta\omega_n - \frac{F_0}{2Hr})X_2 - \omega_n^2 X_1 + \Delta u$

Then arrange it in the form State Equation ($\dot{X}(t)=Ax(t)+B\Delta u(t)$)

$$\begin{bmatrix} \dot{X}_1 \\ \dot{X}_2 \end{bmatrix} = \begin{bmatrix} 0 & 1 \\ -\omega_n^2 & -(2\zeta\omega_n - \frac{F_0}{2Hr}) \end{bmatrix} \begin{bmatrix} X_1 \\ X_2 \end{bmatrix} + \begin{bmatrix} 0 \\ 1 \end{bmatrix} \Delta u. \qquad (3.3.27)$$

Laplace transform for Eq. (3.3.27) can be represented as follows,

From $\dot{X}(t)=Ax(t)+B\Delta u(t)$

Laplace transform $sX(s)=AX(s)+B\Delta U(s)$

$X(s)=(sI-A)^{-1} B\Delta U(s)$,

where $\Delta U(s) = \frac{\Delta u}{s}$,

$$X(s) = \frac{\begin{bmatrix} s + (2\zeta\omega_n - \frac{F_0}{2Hr}) & 1 \\ -\omega_n^2 & s \end{bmatrix} \begin{bmatrix} 0 \\ 1 \end{bmatrix} \frac{\Delta u}{s}}{s^2 + (2\zeta\omega_n - \frac{F_0}{2Hr})s + \omega_n^2}, \qquad (3.3.28)$$

$$\Delta\delta(s) = \frac{\Delta u}{s^2 + (2\zeta\omega_n - \frac{F_0}{2Hr})s + \omega_n^2}, \qquad (3.3.29)$$

$$\Delta\omega(s) = \frac{\Delta u}{s(s^2 + (2\zeta\omega_n - \frac{F_0}{2Hr})s + \omega_n^2)}. \tag{3.3.30}$$

In this thesis, Matlab is used to find the Laplace inverse for the final answer can be expressed as,

$$\Delta\delta = \frac{\Delta u}{\omega_n^2}(1 - \frac{1}{\sqrt{\frac{F_0^2}{16} - (\frac{F_0\zeta K}{2}) + K^2\zeta^2 - K^2}} e^{(\frac{F_0 - 4\zeta K}{4Hr})t}(\cosh(\frac{t\sqrt{\frac{F_0^2}{16} - (\frac{F_0\zeta K}{2}) + K^2\zeta^2 - K^2}}{Hr}) +$$

$$(Hr\sinh(\frac{t\sqrt{\frac{F_0^2}{16} - (\frac{F_0\zeta K}{2}) + K^2\zeta^2 - K^2}}{Hr})(\frac{F_0 - 4\zeta K}{4Hr} - (\frac{\Delta u F_0 - 4\Delta u\zeta K}{2\Delta u Hr}))))), \tag{3.3.31}$$

$$\Delta\omega = \frac{4\Delta u Hr}{\sqrt{F_0^2 - 8F_0\zeta K + 16\zeta^2K^2 - 16K^2}} e^{(\frac{F_0 - 4\zeta K}{4Hr})t} \sinh(\frac{t\sqrt{F_0^2 - 8F_0\zeta K + 16\zeta^2K^2 - 16K^2}}{4Hr}), \tag{3.3.32}$$

where $K = \omega_n Hr$.

Finally, Eq. (3.3.3) and Eq. (3.3.32) is reflecting the effect on the angular frequency and power angle. In this section, a mathematical model is presented to determine the situation for analyzing the effects of frequency.

CHAPTER 4

RESULT AND DISCUSSION

4.1 Introduction

This section presents the simulation results of changing the operating mode of the microgrid under various conditions. 4.2 presents a model of the simulation scenario. and 4.3 presented the simulation results under different circumstances.

In the experiment, all the answers from the mathematical model were calculated with Matlab program.

4.2 Model and circumstances for simulation

This thesis is proposed to test with two systems as follows:

System one: The modified IEEE radial distribution 33-bus test system

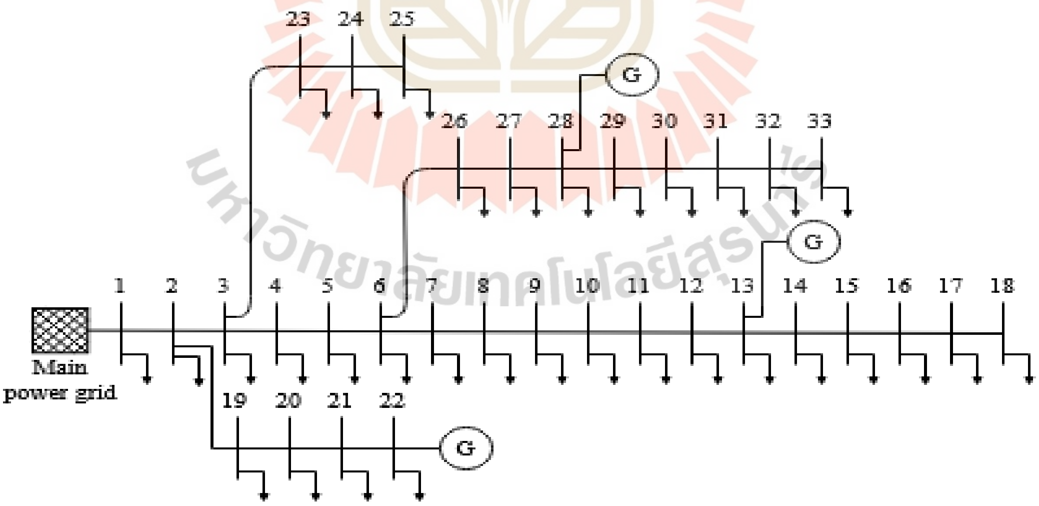

Figure 4.1 Modified IEEE radial distribution system 33-bus

The test system model was modified from IEEE radial distribution 33-bus (P. Díaz, M. P. Cisneros, E. Cuevas, O. Camarena, F. Fausto and A. González, 2018, V. Vita, 2017 and M. Mousavi, A. M. Ranjbar, A. Safdarian, 2017) by placing the generators at bus 13, 22 and 28, while bus 1 is connected to the MPG as show in Figure 4.1. The generation placement in the test system is resulted from total power loss and generation cost minimization (M. Mousavi, A. M. Ranjbar, A. Safdarian, 2017). There are two scenarios in this test system:

Scenario 1: MPG disconnected while MG is receiving electric power.

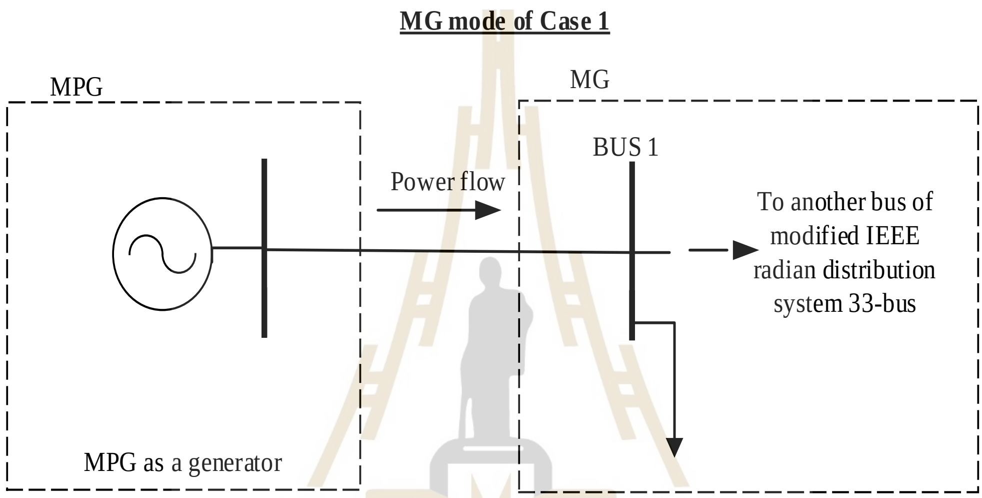

Figure 4.2 Scenario 1 MG is receiving electric power

This situation when the MPG is disconnected while the MG receives the input power from the MPG is shown in Figure 4.2. The participation factor used in the DSLF calculation is shown in Table 4.1.

Table 4.1 Participation factor of Scenario 1

Generator buses	Participation factor
Bus 1 (MPG)	0.06
Bus 13	0.205
Bus 22	0.397
Bus 28	0.338

In the test of disconnection, the power flow from MPG to MG is small. Therefore, from Table 4.1, the power flow from MPG to bus 1 is determined at 6% of Power Generation.

Scenario 2: MPG disconnected while MG is supplying electric power.

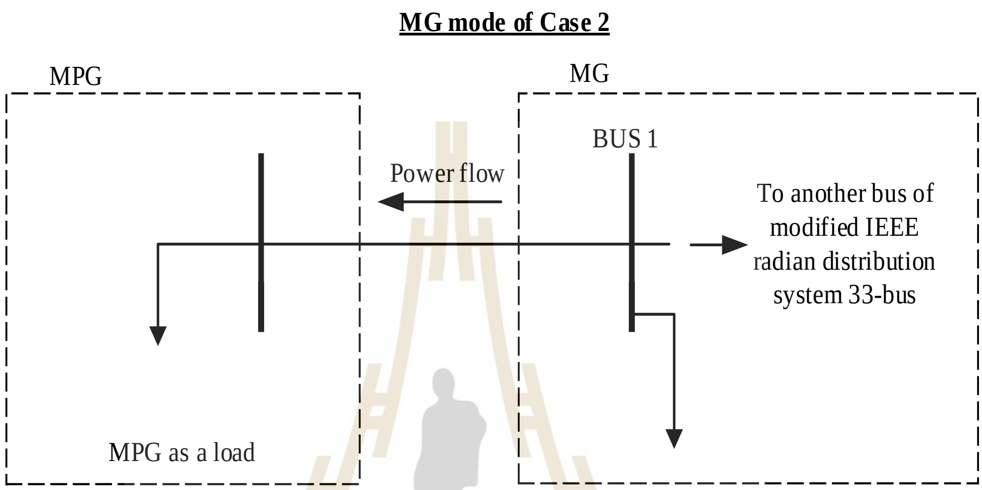

Figure 4.3 Scenario 2 MG is supplying electric power

The opposite of scenario 1 when MPG is disconnected while MG is supplying power to MPG is shown in Figure 4.3.

Table 4.2 Participation factor of Scenario 2

Generator buses	Participation factor
Bus 13	0.218
Bus 22	0.422
Bus 28	0.360

In this situation, the MPG will behave as a load. The power flow from MPG to MG is defined as 100 kW and the participation factor of the other generators is shown in Table 4.2.

System two: The modified IEEE radial distribution 69-bus test system.

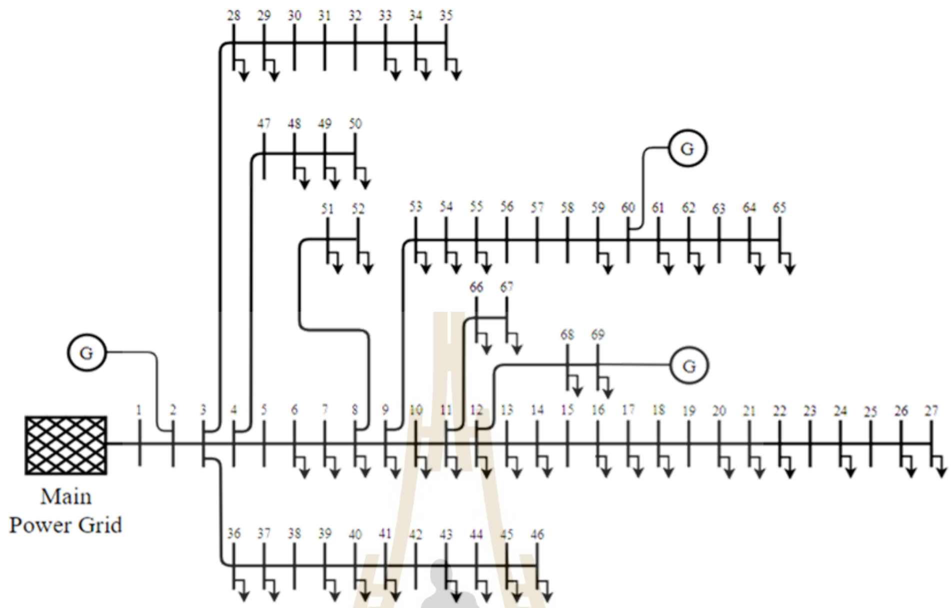

Figure 4.4 Modified IEEE radial distribution system 69-bus

This test system is modified from the IEEE 69 bus system. Modified by placement distributed generator in buses 2, 60 and 69 is shown in Figure 4.4. (P. Díaz, M. P. Cisneros, E. Cuevas, O. Camarena, F. Fausto and A. González, 2017)

Scenario 3: MPG disconnected while MG is receiving electric power.

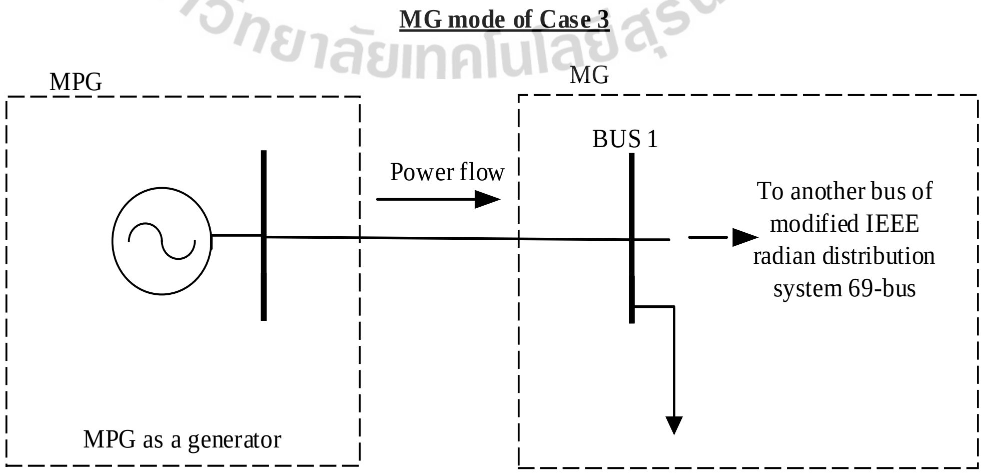

Figure 4.5 Scenario 3 MG is receiving electric power

This scenario is the same as scenario 1. The modified from the IEEE 69 bus system, the test system was analyzed under this scenario.

Table 4.3 Participation factor of Scenario 3

Generator buses	Participation factor
Bus 1 (MPG)	0.060
Bus 2	0.600
Bus 60	0.168
Bus 69	0.171

In Scenario 3 this is similar to Scenario 1. but using the test system as show in Figure 4.4, the participation factor is shown in Table 4.3.

Scenario 4: MPG disconnected while MG is supplying electric power.

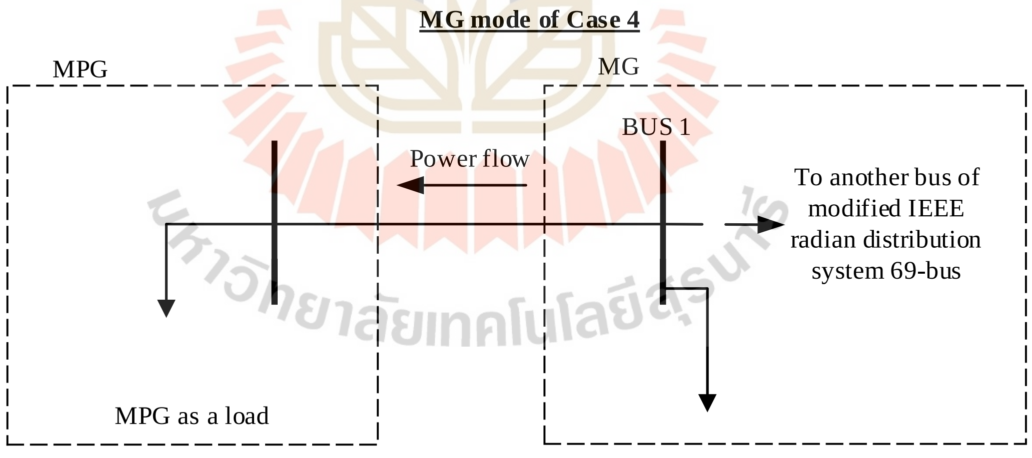

Figure 4.6 Scenario 4 MG is supplying electric power

The same principles and concepts as in scenario 3. In this situation, the test system is the modified from the IEEE 69 bus is shown in Figure 4.6.

Table 4.4 Participation factor of Scenario 4

Generator buses	Participation factor
Bus 2	0.639
Bus 60	0.179
Bus 69	0.182

All example scenarios, the power flow is calculated with a rough estimate of the frequency using the DSLF method.

4.3 Frequency Deviation

In this topic, the results of the experiment on finding the frequency deviation using the method DSLF and the Swing Equation Method under the same situation.

In the simulation of Scenario 1

Determination of the approximate frequency deviation with the test system under scenario 1 in Figure 4.2.

- Using DSLF

In this simulation, the MPG supplies power to MG 228.0 kW before MG is connected. The total power generation including power supply from MPG is 3,715 kW before MG is disconnected and changing the status of MG to islanded mode. The impact on system control both primary and secondary controls.

Table 4.5 Simulation Results of Scenario 1

Power flow (kW)	Before transfer	After transfer	
		Primary control	Secondary control
MPG	228	0	0
P_{G13}	779	779	831.5
P_{G22}	1,508.5	1,508.5	1,588.2
P_{G28}	1,284.3	1,284.3	1,324.9
Power Generation	3,799.8	3,571.8	3,744.6
Power Demand	3,715.0	3,715.0	3,715.0
Power Loss	84.8	-	29.6
Frequency (Hz)	50	49.5963	50

From the experimental results in Table 4.5, the main control power generation was unchanged. But the frequency decreases because the master regulator adjusts the frequency to control the power as in equation (3.2.7). On the other hand, the secondary control frequency is controlled at 50 Hz as it should, but the power generation is reevaluated in response to the load. All generators are adjusted to compensate for lost power generation from the main grid. Total power generation without power supply from MPG is 3,744.6 kW after secondary control operation. Note that the power loss is reduced from 84.8 kW to 29.6 kW due to the increase in the local version. This results in a decrease in overall power generation after transferring the MG mode.

- Using Swing Equation

Parameter adjustment to determine the behavior of changes in the frequency response after system interference. In this test, Scenario 1 was used in the test.

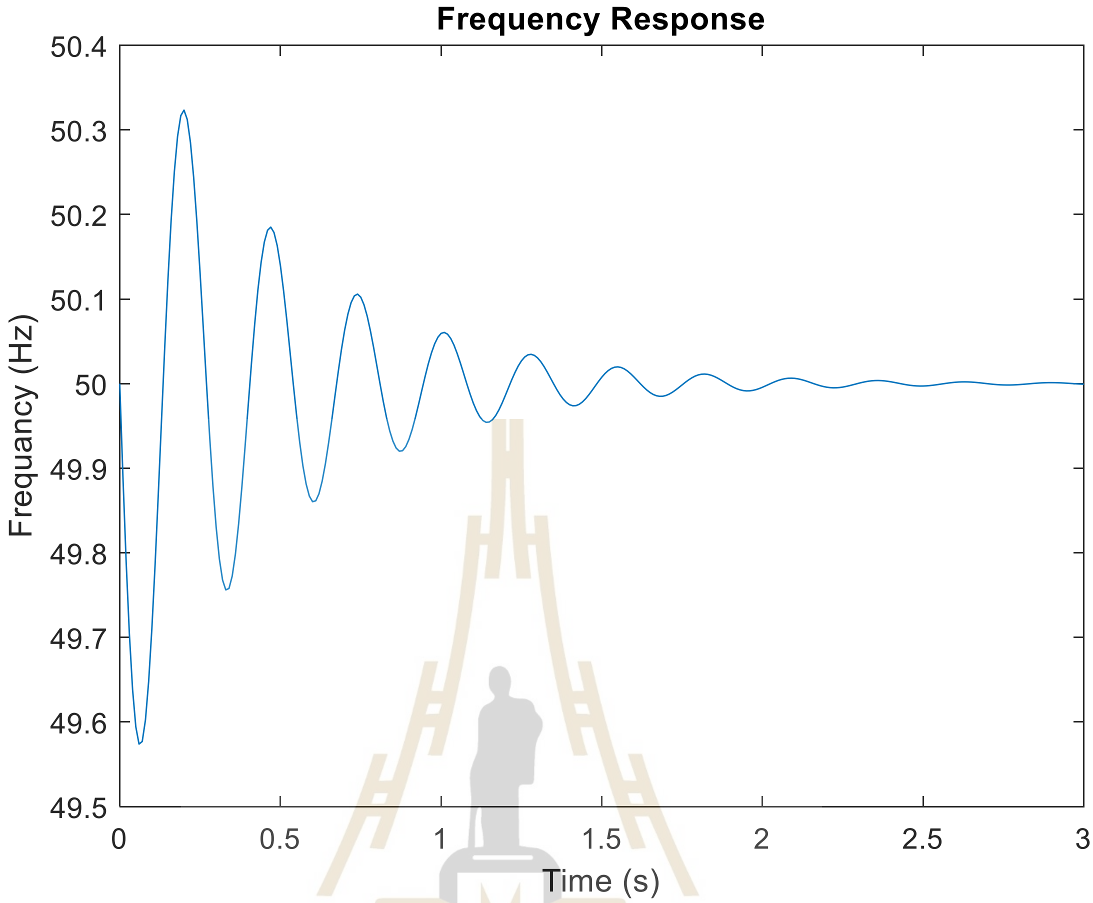

Figure 4.7 Frequency Response of Scenario 1

Figure 4.7 shows the result of adjusting the parameters of swing equation. The adjusted parameters are as $F_0 = 50\ Hz$, $H = 5$, $r = 25$ and $D = 0.138$.

In the simulation of scenario 2

Determination of the approximate frequency deviation with the test system in Figure 4.3 with participation factor in Table 4.2.

- Using DSLF

In Scenario 2, the main power grid receives power from the MG 185.75 kW, in connected mode, before MG is disconnected, changing the status of MG to change to islanded mode. The effect of disconnection on system control both primary and secondary controls are shown in Table 4.6.

Table 4.6 Simulation Result of Scenario 2

Power flow (kW)	Before transfer	After transfer	
		Primary control	Secondary control
MPG	-100	0	0
P_{G13}	837.8	837.8	816.2
P_{G22}	1,621.7	1,621.7	1,579.9
P_{G28}	1,383.5	1,383.5	1,347.8
Power Generation	3,843.0	3,843.0	3,743.9
Power Demand	3,815.0	3,715.0	3,715.0
Power Loss	28.0	-	28.9
Frequency (Hz)	50	50.237	50

From the experimental results in Table 4.6, power generation of primary control has not changed. But the frequency increases to 50.237 Hz, because the primary control will adjust the frequency to control the power, as in Eq. (3.2.7). On the contrary, the power generation of the secondary control is stable at 50 Hz. From the experimental Table 4.6, the secondary control power generation has decreased due to the decrease in the load at the main power grid, resulting in a reduce power generation.

- Using Swing Equation

Parameter adjustment to determine the behavior of changes in the frequency response after system interference. In this test, Scenario 2 was used in the test.

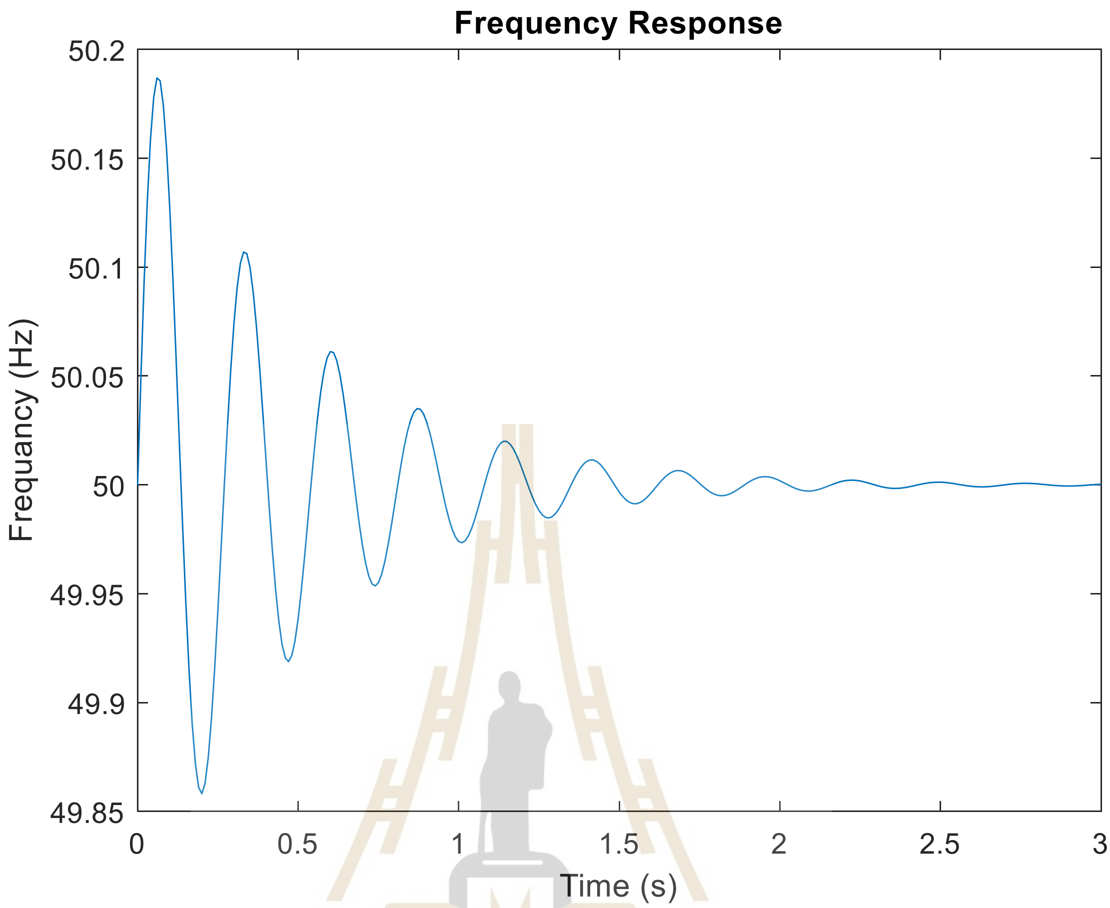

Figure 4.8 Frequency Response of Scenario 2

Figure 4.8 shows the result of adjusting the parameters of swing equation. The adjusted parameters are as $F_0 = 50\ Hz$, $H = 5$, $r = 25$ and $D = 0.138$.

In the simulation of Scenario 3

Determination of the approximate frequency deviation with the test system in Figure 4.5 with participation factor in Table 4.3.

- Using DSLF

while the MPG supplies power to MG 228.0 kW before MG is connected. The total power generation including power supply from MPG is 3,715 kW before MG is disconnected and changing the status of MG to islanded mode. The impact on system control both primary and secondary controls is shown in Table 4.7.

Table 4.7 Simulation Results of Scenario 3

Power flow (kW)	Before transfer	After transfer	
		Primary control	Secondary control
MPG	256.7	0	0
P_{G2}	2,567.2	2,567.2	2,741.3
P_{G60}	720.0	720.0	738.7
P_{G69}	734.4	734.4	750.7
Power Generation	4,278.3	4,021.6	4,230.7
Power Demand	3,801.4	3,801.4	3,801.4
Power Loss	476.9	-	429.3
Frequency (Hz)	50	49.5963	50

From the experimental results in Table 4.6, the main control power generation was unchanged. But the frequency decreases because the master regulator adjusts the frequency to control the power according to Equation (3.2.7). Conversely, the secondary control frequency is regulated at 50 Hz as it should, but the power generation is re-evaluated in response. Responsive to load All generators are adjusted to compensate for lost power generation from the main grid. Total power generation without power supply from MPG is 4,278.3 kW after secondary control operation. Note that the power loss increased from 476.9 kW to 515.7 kW due to the increase in the local version. This results in a decrease in overall power production after transferring MG mode.

- Using Swing Equation

Parameter adjustment to determine the behavior of changes in the frequency response after system interference. In this test, Scenario 3 was used in the test.

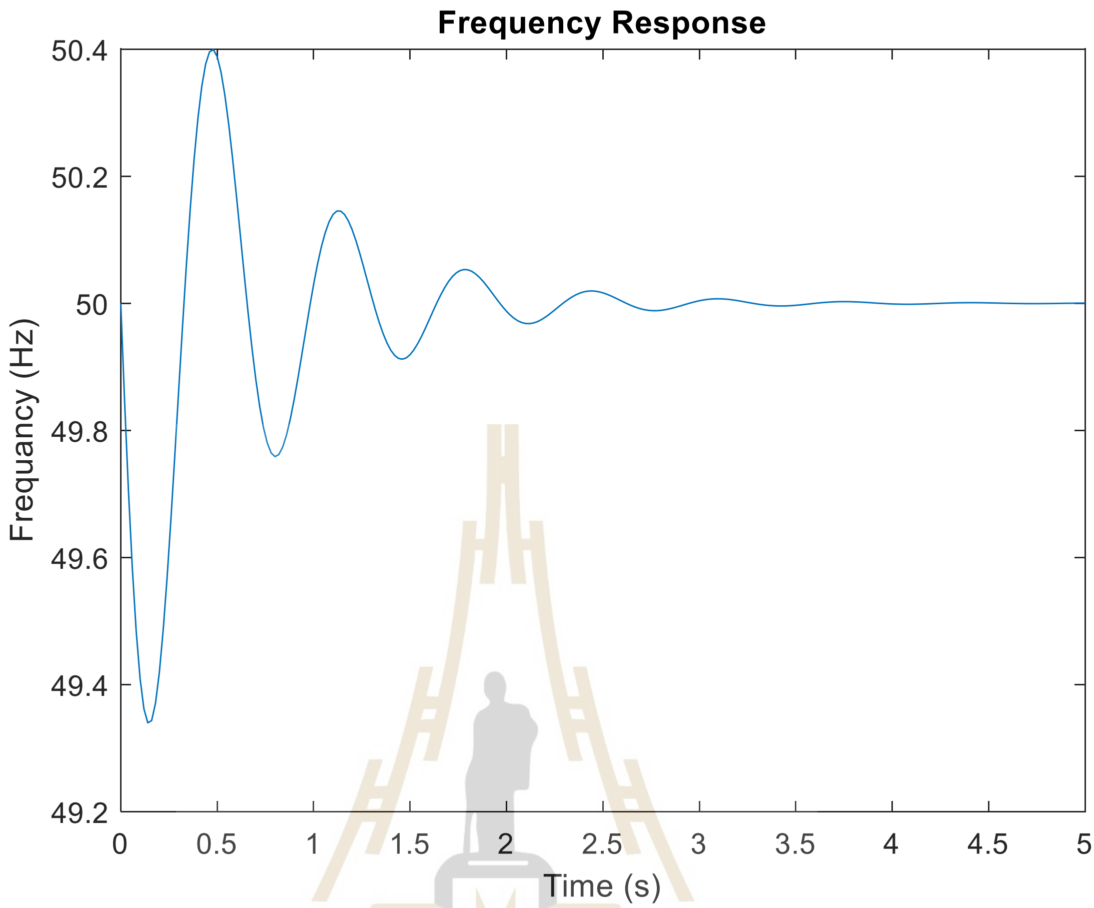

Figure 4.9 Frequency Response of Scenario 3

Figure 4.9 shows the result of adjusting the parameters of swing equation. The adjusted parameters are as $F_0 = 50$ *Hz*, $H = 5$, $r = 25$ and $D = 0.138$.

In the simulation of Scenario 4

Determination of the approximate frequency deviation with the test system in Figure 4.6 with participation factor in Table 4.4.

- Using DSLF

While the MPG powers the MG 228.0 kW before the MG is connected, the total power generation including the power supply from the MPG is 3,715 kW before the MG is disconnected and the MG state is switched to island mode. Control systems for both primary and secondary controls are shown in Table 4.8.

Table 4.8 Simulation Results of Scenario 4

Power flow (kW)	Before transfer	After transfer	
		Primary control	Secondary control
MPG	-100	0	0
P_{G2}	2,749.4	2,749.4	2,693.5
P_{G60}	769.8	769.8	754.2
P_{G69}	783.6	783.6	767.7
Power Generation	4,302.8	4,302.8	4,215.4
Power Demand	3,901.4	3,801.4	3,801.4
Power Loss	401.4	-	414.0
Frequency (Hz)	50	50.1136	50

From the experimental results in Table 4.8, the main control power generation was unchanged. But the frequency decreases because the master regulator adjusts the frequency to control the power as in Eq. (3.2.7). On the other hand, the secondary control frequency is controlled at 50 Hz as it should, but the power generation is reevaluated in response to the load. All generators are adjusted to compensate for lost power generation from the main grid. Total power generation without power supply from MPG is 4,302.8 kW after secondary control operation. Note that the power loss is increase from 401.4 kW to 414.0 kW due to the increase in the local version. This results in a decrease in overall power generation after transferring the MG mode.

- Using Swing Equation

Parameter adjustment to determine the behavior of changes in the frequency response after system interference. In this test, Scenario 4 was used in the test.

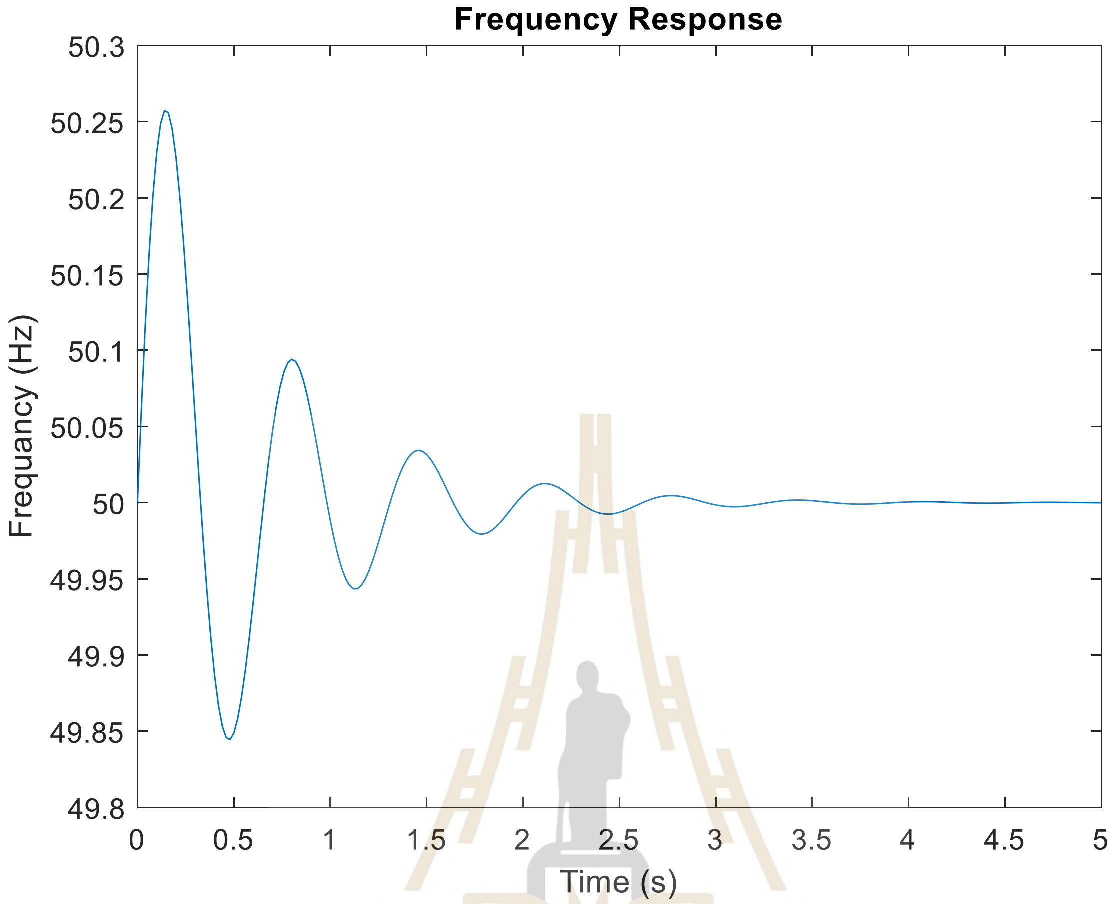

Figure 4.10 Frequency Response of Scenario 4

Figure 4.10 shows the result of adjusting the parameters of swing equation. The adjusted parameters are as $F_0 = 50\ Hz$, $H = 5$, $r = 25$ and $D = 0.138$.

From the experiment to find the solution by using the oscillation equation It was found that the variables were adjusted for calculating the frequency deviation. If the adjusted variables change, the frequency response curve will also change. Therefore, it may affect the discrepancy caused by adjusting the variable. Different from DSLF method that can be calculated more easily. However, DSLF cannot provide a graphical response, therefore DSLF is suitable for initial evaluation of primary frequencies before transfer.

CHAPTER 5

CONCLUSION

5.1 Conclusion

This thesis presents a method for calculating the primary frequency deviation due to the mode transfer of the microgrid system. This is a different calculation from other studies, but the results obtained from this method are quick and uncomplicated. The proposed method is DSLF for frequency Deviation, which is a combination of normal DSLF, and Equation 3.2.7 modified in the jacobian matrix. The results are reliable. and that method was also published at ICPEI 2020.

This thesis also examines swing equation method as a guideline for solving problems when excessive frequency deviations occur in the system. this method was designed and studied considering the simulation of damping and speed droop and when testing parameter adjustments.

5.2 Recommendation for future

Due to the experimental results of adjusting the parameters of the swing equation in item 4.3 showed that the frequency response can be controlled by adjusting the parameters, there are suggestions as follows:

I. Use the optimization method to find the parameters suitable for the system to reduce the occurrence of under-frequency conditions.

REFERENCES

Y. R. Kukandeh and M. H. Kazemi (2018). Microgrid Control in Islanding and Connected Mode. **ICEE., 2018**, DOI. 10.1109/ICEE.2018.8472560.

Q. Fu, A. Nasiri, A. Solanki, A. B. Ahmed, L. Weber, and V. Bhavaraju (2015). Microgrids: Architectures, Controls, Protection, and Demonstration. **Electric Power Components and Systems.** vol.43, no.12, 1453–1465.

M. Prakash.M and J. Paul (2016). Control of Microgrid for Different Modes of Operation. **International Journal of Engineering Research & Technology**. vol. 5, no. 05, pp. 815-820.

J. H. Zheng, Y. T. Wang, Z. J. Wang, S. Zhu, X. Wang and S. Xinwei (2011). Study on microgrid operation modes switching based on eigenvalue analysis. **International Conference on Advanced Power System Automation and Protection.** DOI. 10.1109/APAP.2011.6180443.

L. I. U. Meiyin, L. V. Zhenhua, W. U. Beibei , G. U. O. Chongyang, and H.A.N. Pingping (2018). Research on Switching Model of Microgrid with Distributed Power Supply. **ICSREE**. DOI. 10.1051/e3sconf/20185703008.

T. Wu, Z. Alaywan, and A. D. Papalexopoulos (2005). Locational Marginal Price Calculations Using the Distributed-Slack Power-Flow Formulation. **IEEE TRANSACTIONS ON POWER SYSTEMS**. vol. 20, no. 2, 1188-1190.

P. Yan (2001). Modified Distributed Slack Bus Load Flow Algorithm for Determining Economic Dispatch in Deregulated Power Systems. **PESW**. 1226-1231.

K. Chayakulkheeree (2007). Application of distributed slack bus power flow to competitive environments. **AUPEC**. Paper no.20-16, 531–536.

A. J. Wood, B. F. Wollengerg, G. B. Sheblé (2014). Power Generation, Operation, And control. vol. 3rd, Canada, John Wiley & Sons.

P. Díaz, M. P. Cisneros, E. Cuevas, O. Camarena, F. Fausto and A. González (2018). A Swarm Approach for Improving Voltage Profiles and Reduce Power Loss on Electrical Distribution Networks. **IEEE Access**, vol. 6, 49498-49512.

V. Vita, “Development of a Decision-Making Algorithm for the Optimum Size and Placement of Distributed Generation Units in Distribution Networks, **Energies**, vol. 10, pp. 1433-1446, 2017.

M. Mousavi, A. M. Ranjbar, A. Safdarian (2017). Optimal DG Placement and Sizing Based on MICP in Radial Distribution Networks. **Smart Grid Conference (SGC)**.

Yasser R. K. and Mohammad H. K., (2018). Microgrid Control In Islanding And Connected Mode. **Iranian Conference on Electrical Engineering**.

D. Leng and S. Polmai, (2019). Transient Respond Comparison Between ModifiedDroop Control and Virtual Synchronous Generatorin Standalone Microgrid. **International Conference on Engineering, Applied Sciences and Technology (ICEAST).** DOI: 10.1109/ICEAST.2019.8802552.

S. Mansour, M. I. Marei and A. A. Sattar, (2016). Droop based Control Strategy for a Microgrid. **Global Journal of Researches in Engineering: F Electrical and Electronics Engineering.** Vol 16, Issue 7, V. 1.0.

Qiang F., Adel N., Ashishkumar S., Abedalsalam B. A., Luke W., and Vijay B., (2015). Microgrids: Architectures, Controls, Protection, and Demonstration. **Electric Power Components and Systems**. 43(12), 1453–1465.

Megha Prakash.M. and Jasmy P., (2016). Control of Microgrid for Different Modes of Operation. **International Journal of Engineering Research & Technology (IJERT).** Vol. 5 Issue 05, 2278-0181.

M. Yang, X. Hongliang, B. Chunyan, W. Shengyi, Z. Han, J. Yuanwei, (2016). Study on Smooth Switching of Microgrid Operation States Using Sliding Mode Control. **Chinese Control and Decision Conference (CCDC)**. 28th, 6105-6108.

Z. Xiaobo and Z. Baohui, (2014). Improved microgrid energy storage device model in microgrid mode switching process. **International Conference on Green Energy (ICGE)**. 1st, 96-100.

APPENDIX I

Data of Test Systems

Appendix A1: the modified IEEE radial distribution 33-bus system

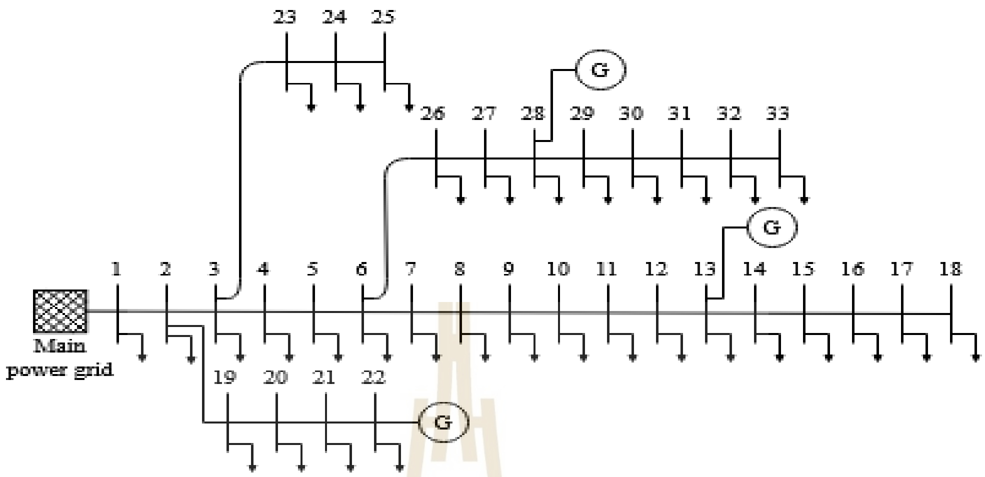

Figure A1.1 Modified IEEE radial distribution 33-bus system

Table A1.1 Transmission Line Data for Modified IEEE radial distribution 33-bus system

From Bus	To Bus	R(P.U.)	X(P.U.)	TAP	MVA Line
1	2	0.0575	0.0298	0	85
2	3	0.3076	0.1567	0	85
3	4	0.2284	0.1163	0	85
4	5	0.2378	0.1211	0	85
5	6	0.511	0.4411	0	85
6	7	0.1168	0.3861	0	85
7	8	1.0678	0.7706	0	85
8	9	0.6426	0.4617	0	85
9	10	0.6489	0.4617	0	85
10	11	0.1227	0.0406	0	85
11	12	0.2336	0.0772	0	85
12	13	0.9159	0.7206	0	85

Table A1.1 Transmission Line Data for Modified IEEE radial distribution 33-bus system (Continued)

From Bus	To Bus	R(P.U.)	X(P.U.)	TAP	MVA Line
13	14	0.3379	0.4448	0	85
14	15	0.3687	0.3282	0	85
15	16	0.4656	0.34	0	85
16	17	0.8042	1.0738	0	85
17	18	0.4567	0.3581	0	85
2	19	0.1023	0.0976	0	85
19	20	0.9385	0.8457	0	85
20	21	0.2555	0.2985	0	85
21	22	0.4423	0.5848	0	85
3	23	0.2815	0.1924	0	85
23	24	0.5603	0.4424	0	85
24	25	0.559	0.4374	0	85
6	26	0.1267	0.0645	0	85
26	27	0.1773	0.0903	0	85
27	28	0.6607	0.5826	0	85
28	29	0.5018	0.4371	0	85
29	30	0.3166	0.1613	0	85
30	31	0.608	0.6008	0	85
31	32	0.1937	0.2258	0	85

Table A1.2 Bus Data for Modified IEEE radial distribution 33-bus system

Bus No.	Bus Type	P_{LOAD}	Q_{LOAD}	Participation factor
1	Gen	0	0	0.06
2	Load	0.1	0.06	0
3	Load	0.09	0.04	0
4	Load	0.12	0.08	0
5	Load	0.06	0.03	0
6	Load	0.06	0.02	0
7	Load	0.2	0.1	0
8	Load	0.2	0.1	0
9	Load	0.06	0.02	0
10	Load	0.06	0.02	0
11	Load	0.045	0.03	0
12	Load	0.06	0.035	0
13	Gen	0.06	0.035	0.205
14	Load	0.12	0.08	0
15	Load	0.06	0.01	0
16	Load	0.06	0.02	0
17	Load	0.06	0.02	0
18	Load	0.09	0.04	0
19	Load	0.09	0.04	0
20	Load	0.09	0.04	0
21	Load	0.09	0.04	0
22	Gen	0.09	0.04	0.397
23	Load	0.09	0.05	0
24	Load	0.42	0.2	0
25	Load	0.42	0.2	0
26	Load	0.06	0.025	0

Table A1.2 Bus Data for Modified IEEE radial distribution 33-bus system (Continued)

Bus No.	Bus Type	P_{LOAD}	Q_{LOAD}	Participation factor
27	Load	0.06	0.025	0
28	Gen	0.06	0.02	0.338
29	Load	0.12	0.07	0
30	Load	0.2	0.6	0
31	Load	0.15	0.07	0
32	Load	0.21	0.1	0
33	Load	0.06	0.04	0

Table A1.3 Result of Power Flow using DSLF from Modified IEEE radial distribution 33-bus system

No. Bus	Bus Type	|V| (p.u.)	DEL (deg)	P_{gen} (MW)	Q_{gen} (MVar)	P_{Load} (MW)	Q_{Load} (MVar)
1	Gen	1.0000	0.0000	0.2280	0.3019	0.0000	0.0000
2	Load	0.9993	0.1831	0.0000	0.0000	0.1000	0.0600
3	Load	0.9947	0.1552	0.0000	0.0000	0.0900	0.0400
4	Load	0.9942	0.1457	0.0000	0.0000	0.1200	0.0800
5	Load	0.9940	0.1276	0.0000	0.0000	0.0600	0.0300
6	Load	0.9941	0.0863	0.0000	0.0000	0.0600	0.0200
7	Load	0.9933	-0.0978	0.0000	0.0000	0.2000	0.1000
8	Load	0.9921	-0.1996	0.0000	0.0000	0.2000	0.1000
9	Load	0.9931	-0.2096	0.0000	0.0000	0.0600	0.0200
10	Load	0.9946	-0.1939	0.0000	0.0000	0.0600	0.0200
11	Load	0.9949	-0.2045	0.0000	0.0000	0.0450	0.0300
12	Load	0.9957	-0.2311	0.0000	0.0000	0.0600	0.0350
13	Gen	1.0000	-0.1152	0.7790	1.0314	0.0600	0.0350

Table A1.3 Result of Power Flow using DSLF from Modified IEEE radial distribution 33-bus system (Continued)

No. Bus	Bus Type	|V| (p.u.)	DEL (deg)	P_{gen} (MW)	Q_{gen} (MVar)	P_{Load} (MW)	Q_{Load} (MVar)
14	Load	0.9979	-0.3232	0.0000	0.0000	0.1200	0.0800
15	Load	0.9966	-0.4228	0.0000	0.0000	0.0600	0.0100
16	Load	0.9954	-0.4842	0.0000	0.0000	0.0600	0.0200
17	Load	0.9935	-0.6882	0.0000	0.0000	0.0600	0.0200
18	Load	0.9930	-0.7135	0.0000	0.0000	0.0900	0.0400
19	Load	0.9992	0.6062	0.0000	0.0000	0.0900	0.0400
20	Load	1.0003	4.4547	0.0000	0.0000	0.0900	0.0400
21	Load	1.0002	5.6795	0.0000	0.0000	0.0900	0.0400
22	Gen	1.0000	8.0227	1.5085	1.9974	0.0900	0.0400
23	Load	0.9912	0.0609	0.0000	0.0000	0.0900	0.0500
24	Load	0.9846	-0.2093	0.0000	0.0000	0.4200	0.2000
25	Load	0.9814	-0.3424	0.0000	0.0000	0.4200	0.2000
26	Load	0.9947	0.0868	0.0000	0.0000	0.0600	0.0250
27	Load	0.9956	0.0892	0.0000	0.0000	0.0600	0.0250
28	Gen	1.0000	0.3129	1.2843	1.7006	0.0600	0.0200
29	Load	0.9924	0.5247	0.0000	0.0000	0.1200	0.0700
30	Load	0.9891	0.8101	0.0000	0.0000	0.2000	0.6000
31	Load	0.9853	0.5814	0.0000	0.0000	0.1500	0.0700
32	Load	0.9844	0.5191	0.0000	0.0000	0.2100	0.1000
33	Load	0.9841	0.4981	0.0000	0.0000	0.0600	0.0400

Appendix A2: the modified IEEE radial distribution 69-bus system

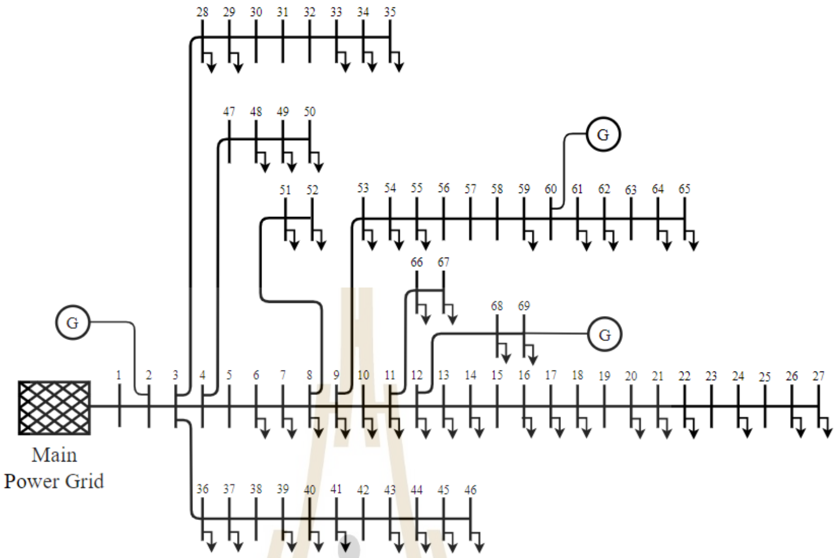

Figure B1.1 Modified IEEE radial distribution 69-bus system

Table B1.1 Transmission Line Data for Modified IEEE radial distribution 69-bus system

From Bus	To Bus	R(P.U.)	X(P.U.)	TAP	MVA Line
1	2	0.00031	0.00075	0	100
2	3	0.00031	0.00075	0	100
3	4	0.00094	0.00225	0	100
4	5	0.01566	0.01834	0	100
5	6	0.22836	0.11630	0	100
6	7	0.23772	0.12110	0	100
7	8	0.05753	0.03000	0	100
8	9	0.03076	0.02000	0	100
9	10	0.51099	0.16890	0	100
10	11	0.11680	0.03862	0	100

Table B1.1 Transmission Line Data for Modified IEEE radial distribution 69-bus system (Continued)

From Bus	To Bus	R(P.U.)	X(P.U.)	TAP	MVA Line
11	12	0.44386	0.14668	0	100
12	13	0.64264	0.21213	0	100
13	14	0.65138	0.21213	0	100
14	15	0.66011	0.21812	0	100
15	16	0.12266	0.04056	0	100
16	17	0.23360	0.07724	0	100
17	18	0.00293	0.00100	0	100
18	19	0.20440	0.06757	0	100
19	20	0.13140	0.04305	0	100
20	21	0.21313	0.07044	0	100
21	22	0.00873	0.00287	0	100
22	23	0.09927	0.03282	0	100
23	24	0.21607	0.07144	0	100
24	25	0.46720	0.15442	0	100
25	26	0.19273	0.06370	0	100
26	27	0.10806	0.03569	0	100
3	28	0.00275	0.00674	0	100
28	29	0.03993	0.09764	0	100
29	30	0.24820	0.08205	0	100
30	31	0.04380	0.01448	0	100
31	32	0.21900	0.07238	0	100
32	33	0.52347	0.17570	0	100
33	34	1.06566	0.35227	0	100
34	35	0.91967	0.30404	0	100
3	36	0.00275	0.00674	0	100
36	37	0.03993	0.09764	0	100

Table B1.1 Transmission Line Data for Modified IEEE radial distribution 69-bus system (Continued)

From Bus	To Bus	R(P.U.)	X(P.U.)	TAP	MVA Line
37	38	0.06570	0.07674	0	100
38	39	0.01897	0.02215	0	100
39	40	0.00112	0.00131	0	100
40	41	0.45440	0.53090	0	100
41	42	0.19342	0.22605	0	100
42	43	0.02558	0.02982	0	100
43	44	0.00574	0.00724	0	100
44	45	0.06795	0.08566	0	100
4	46	0.00056	0.00075	0	100
46	47	0.00212	0.00524	0	100
47	48	0.05310	0.12996	0	100
48	49	0.18081	0.44243	0	100
8	50	0.05129	0.12547	0	100
50	51	0.05790	0.02951	0	100
9	52	0.20708	0.07113	0	100
52	53	0.10856	0.05528	0	100
53	54	0.12666	0.06451	0	100
54	55	0.17732	0.09028	0	100
55	56	0.17551	0.08941	0	100
56	57	0.99204	0.33299	0	100
57	58	0.48897	0.16409	0	100
58	59	0.18980	0.00628	0	100
59	60	0.24090	0.07312	0	100
60	61	0.31664	0.16128	0	100
61	62	0.06077	0.03095	0	100
62	63	0.09047	0.04605	0	100

Table B1.1 Transmission Line Data for Modified IEEE radial distribution 69-bus system (Continued)

From Bus	To Bus	R(P.U.)	X(P.U.)	TAP	MVA Line
63	64	0.44330	0.22580	0	100
64	65	0.64951	0.33081	0	100
11	66	0.12553	0.03812	0	100
66	67	0.00293	0.00087	0	100
12	68	0.46133	0.15249	0	100
68	69	0.00293	0.00100	0	100

Table B1.2 Bus Data for Modified IEEE radial distribution 69-bus system

Bus No.	Bus Type	P_{LOAD}	Q_{LOAD}	Participation factor
1	Gen	0.00000	0.00000	0.060
2	Gen	0.00000	0.00000	0.600
3	Load	0.00000	0.00000	0.000
4	Load	0.00000	0.00000	0.000
5	Load	0.00000	0.00000	0.000
6	Load	0.00260	0.00220	0.000
7	Load	0.04040	0.03000	0.000
8	Load	0.07500	0.05400	0.000
9	Load	0.03000	0.02200	0.000
10	Load	0.02800	0.01900	0.000
11	Load	0.14500	0.10400	0.000
12	Load	0.14500	0.10400	0.000
13	Load	0.00800	0.00500	0.000
14	Load	0.00800	0.00500	0.000
15	Load	0.00000	0.00000	0.000
16	Load	0.04500	0.03000	0.000

Table B1.2 Bus Data for Modified IEEE radial distribution 69-bus system (Continued)

Bus No.	Bus Type	P_{LOAD}	Q_{LOAD}	Participation factor
17	Load	0.06000	0.03500	0.000
18	Load	0.06000	0.03500	0.000
19	Load	0.00000	0.00000	0.000
20	Load	0.00100	0.00060	0.000
21	Load	0.11400	0.08100	0.000
22	Load	0.00500	0.00350	0.000
23	Load	0.00000	0.00000	0.000
24	Load	0.02800	0.02000	0.000
25	Load	0.00000	0.00000	0.000
26	Load	0.01400	0.01000	0.000
27	Load	0.01400	0.01000	0.000
28	Load	0.02600	0.01860	0.000
29	Load	0.02600	0.01860	0.000
30	Load	0.00000	0.00000	0.000
31	Load	0.00000	0.00000	0.000
32	Load	0.00000	0.00000	0.000
33	Load	0.01400	0.01000	0.000
34	Load	0.01950	0.01400	0.000
35	Load	0.00600	0.00400	0.000
36	Load	0.02600	0.01855	0.000
37	Load	0.02600	0.01855	0.000
38	Load	0.00000	0.00000	0.000
39	Load	0.02400	0.01700	0.000
40	Load	0.02400	0.01700	0.000
41	Load	0.00120	0.00100	0.000
42	Load	0.00000	0.00000	0.000

Table B1.2 Bus Data for Modified IEEE radial distribution 69-bus system (Continued)

Bus No.	Bus Type	P_{LOAD}	Q_{LOAD}	Participation factor
43	Load	0.00600	0.00430	0.000
44	Load	0.00000	0.00000	0.000
45	Load	0.03922	0.02630	0.000
46	Load	0.03922	0.02630	0.000
47	Load	0.00000	0.00000	0.000
48	Load	0.07900	0.05640	0.000
49	Load	0.38470	0.27450	0.000
50	Load	0.38470	0.27450	0.000
51	Load	0.04050	0.02830	0.000
52	Load	0.00360	0.00270	0.000
53	Load	0.00435	0.00350	0.000
54	Load	0.02640	0.01900	0.000
55	Load	0.02400	0.01720	0.000
56	Load	0.00000	0.00000	0.000
57	Load	0.00000	0.00000	0.000
58	Load	0.00000	0.00000	0.000
59	Load	0.10000	0.07200	0.000
60	Gen	0.00000	0.00000	0.168
61	Load	1.24400	0.88800	0.000
62	Load	0.03200	0.02300	0.000
63	Load	0.00000	0.00000	0.000
64	Load	0.22700	0.16200	0.000
65	Load	0.05900	0.04200	0.000
66	Load	0.01800	0.01300	0.000
67	Load	0.01800	0.01300	0.000
68	Load	0.02800	0.02000	0.000

Table B1.2 Bus Data for Modified IEEE radial distribution 69-bus system (Continued)

Bus No.	Bus Type	P_{LOAD}	Q_{LOAD}	Participation factor
69	Gen	0.02800	0.02000	0.172

Table B1.3 Result of Power Flow using DSLF from Modified IEEE radial distribution 69-bus system

No. Bus	Bus Type	|V| (p.u.)	DEL (deg)	P_{gen} (MW)	Q_{gen} (MVar)	P_{Load} (MW)	Q_{Load} (MVar)
1	Gen	1.0000	0.0000	0.2567	-0.1069	0.0000	0.0000
2	Gen	1.0000	-0.0004	2.5672	-1.0696	0.0000	0.0000
3	Load	1.0000	-0.0054	0.0000	0.0000	0.0000	0.0000
4	Load	1.0000	-0.0198	0.0000	0.0000	0.0000	0.0000
5	Load	1.0000	-0.1647	0.0000	0.0000	0.0000	0.0000
6	Load	0.9987	-1.7163	0.0000	0.0000	0.0026	0.0022
7	Load	0.9972	-3.3368	0.0000	0.0000	0.0404	0.0300
8	Load	0.9969	-3.7331	0.0000	0.0000	0.0750	0.0540
9	Load	0.9970	-3.9610	0.0000	0.0000	0.0300	0.0220
10	Load	0.9963	-3.6678	0.0000	0.0000	0.0280	0.0190
11	Load	0.9961	-3.6028	0.0000	0.0000	0.1450	0.1040
12	Load	0.9966	-3.4121	0.0000	0.0000	0.1450	0.1040
13	Load	0.9938	-3.2757	0.0000	0.0000	0.0080	0.0050
14	Load	0.9910	-3.1376	0.0000	0.0000	0.0080	0.0050
15	Load	0.9882	-3.0017	0.0000	0.0000	0.0000	0.0000
16	Load	0.9877	-2.9764	0.0000	0.0000	0.0450	0.0300
17	Load	0.9869	-2.9346	0.0000	0.0000	0.0600	0.0350
18	Load	0.9869	-2.9342	0.0000	0.0000	0.0600	0.0350
19	Load	0.9864	-2.9090	0.0000	0.0000	0.0000	0.0000

Table B1.3 Result of Power Flow using DSLF from Modified IEEE radial distribution 69-bus system (Continued)

No. Bus	Bus Type	|V| (p.u.)	DEL (deg)	P_{gen} (MW)	Q_{gen} (MVar)	P_{Load} (MW)	Q_{Load} (MVar)
20	Load	0.9861	-2.8927	0.0000	0.0000	0.0010	0.0006
21	Load	0.9857	-2.8665	0.0000	0.0000	0.1140	0.0810
22	Load	0.9857	-2.8661	0.0000	0.0000	0.0050	0.0035
23	Load	0.9856	-2.8622	0.0000	0.0000	0.0000	0.0000
24	Load	0.9854	-2.8536	0.0000	0.0000	0.0280	0.0200
25	Load	0.9853	-2.8443	0.0000	0.0000	0.0000	0.0000
26	Load	0.9852	-2.8405	0.0000	0.0000	0.0140	0.0100
27	Load	0.9852	-2.8394	0.0000	0.0000	0.0140	0.0100
28	Load	1.0000	-0.0062	0.0000	0.0000	0.0260	0.0186
29	Load	0.9999	-0.0143	0.0000	0.0000	0.0260	0.0186
30	Load	0.9998	-0.0077	0.0000	0.0000	0.0000	0.0000
31	Load	0.9998	-0.0065	0.0000	0.0000	0.0000	0.0000
32	Load	0.9997	-0.0007	0.0000	0.0000	0.0000	0.0000
33	Load	0.9994	0.0132	0.0000	0.0000	0.0140	0.0100
34	Load	0.9991	0.0315	0.0000	0.0000	0.0195	0.0140
35	Load	0.9990	0.0348	0.0000	0.0000	0.0060	0.0040
36	Load	1.0000	-0.0067	0.0000	0.0000	0.0260	0.0186
37	Load	0.9999	-0.0218	0.0000	0.0000	0.0260	0.0186
38	Load	0.9998	-0.0270	0.0000	0.0000	0.0000	0.0000
39	Load	0.9997	-0.0285	0.0000	0.0000	0.0240	0.0170
40	Load	0.9997	-0.0286	0.0000	0.0000	0.0240	0.0170
41	Load	0.9993	-0.0471	0.0000	0.0000	0.0012	0.0010
42	Load	0.9992	-0.0548	0.0000	0.0000	0.0000	0.0000
43	Load	0.9992	-0.0558	0.0000	0.0000	0.0060	0.0043
44	Load	0.9992	-0.0561	0.0000	0.0000	0.0000	0.0000

Table B1.3 Result of Power Flow using DSLF from Modified IEEE radial distribution 69-bus system (Continued)

No. Bus	Bus Type	|V| (p.u.)	DEL (deg)	P_{gen} (MW)	Q_{gen} (MVar)	P_{Load} (MW)	Q_{Load} (MVar)
45	Load	0.9991	-0.0589	0.0000	0.0000	0.0392	0.0263
46	Load	1.0000	-0.0201	0.0000	0.0000	0.0392	0.0263
47	Load	1.0000	-0.0232	0.0000	0.0000	0.0000	0.0000
48	Load	0.9993	-0.0998	0.0000	0.0000	0.0790	0.0564
49	Load	0.9974	-0.3167	0.0000	0.0000	0.3847	0.2745
50	Load	0.9963	-3.8014	0.0000	0.0000	0.3847	0.2745
51	Load	0.9962	-3.8006	0.0000	0.0000	0.0405	0.0283
52	Load	0.9966	-5.4493	0.0000	0.0000	0.0036	0.0027
53	Load	0.9971	-6.2742	0.0000	0.0000	0.0044	0.0035
54	Load	0.9977	-7.2359	0.0000	0.0000	0.0264	0.0190
55	Load	0.9986	-8.5820	0.0000	0.0000	0.0240	0.0172
56	Load	0.9996	-9.9135	0.0000	0.0000	0.0000	0.0000
57	Load	1.0000	-17.0488	0.0000	0.0000	0.0000	0.0000
58	Load	1.0000	-20.5601	0.0000	0.0000	0.0000	0.0000
59	Load	0.9994	-21.8193	0.0000	0.0000	0.1000	0.0720
60	Gen	1.0000	-23.5530	0.7200	-0.3000	0.0000	0.0000
61	Load	0.9932	-23.3705	0.0000	0.0000	1.2440	0.8880
62	Load	0.9930	-23.3633	0.0000	0.0000	0.0320	0.0230
63	Load	0.9926	-23.3537	0.0000	0.0000	0.0000	0.0000
64	Load	0.9909	-23.3065	0.0000	0.0000	0.2270	0.1620
65	Load	0.9903	-23.2923	0.0000	0.0000	0.0590	0.0420
66	Load	0.9961	-3.5994	0.0000	0.0000	0.0180	0.0130
67	Load	0.9961	-3.5994	0.0000	0.0000	0.0180	0.0130
68	Load	1.0000	-3.3584	0.0000	0.0000	0.0280	0.0200
69	Gen	1.0000	-3.3581	0.7344	-0.3060	0.0280	0.0200

APPENDIX II

List of Publications

List of Publication

Keerati Chayakulkheeree Nithiwat Intharasomchai and Udoum Chhor, (2019). Probabilistic Day-Ahead Optimal Power Dispatch Using Truncated Normal Density Function Considering Price-Based Real-Time Demand Response. **Electrical Engineering Conference 42 (EECON 42)**, PW14.

Nithiwat Intharasomchai and Keerati Chayakulkheeree, (2020) Steady State Primary Frequency Estimation for Microgrid Transferring Mode Using Distributed Slack Bus Load Flow Analysis. **2020 International Conference on Power, Energy and Innovations (ICPEI 2020)**, 101 - 104.

Probabilistic Day-Ahead Optimal Power Dispatch Using Truncated Normal Density Function Considering Price-Based Real-Time Demand Response

Keerati Chayakulkheeree[1] Nithiwat Intharasomchai[1] and Udoum Chhor[2]

[1]School of Electrical Engineering, Institute of Engineering,
Suranaree University of Technology, Thailand, keerati.ch@sut.ac.th,
[2]Department of Electrical Engineering, Faculty of Engineering,
National Polytechnic Institute of Cambodia, Phnom Penh, Cambodia

Abstract

In this paper, a probabilistic day-ahead optimal power dispatch (PDOPD) using truncated normal probability density function (TNPDFF) has been proposed to solve the power generation dispatching with the price-based real-time demand response (PRDR). The PDOPD has been solved using linear programming (LP) based Monte Carlo Simulation (MCS). The simulation result has prosperously shown that the proposed method can handle the optimal solutions for real power dispatch considering PRDR, with probobilistic load consideration. Therefore, the proposed method can efficiently and effectively minimize total power generation cost, while trading off PRDR cost in the optimal power dispatch problem, considering load uncertainty.

Keywords: probabilistic day-ahead optimal power dispatch, truncated normal probability density function, price-based real-time demand response.

1. Introduction

Recently, the day-ahead optimal power dispatch in the emerging more marketing-based power system has become one of the most extensive optimization tools required in the power system planning and operation. With the above issues, many researchers have studied optimization techniques to investigate the power system. Many optimization algorithms have always been mentioned both artificial intelligence and conventional methods to obtain an optimal operation for the recent increasing more complex power systems.

Meanwhile, the accurate daily load forecasts for now-a-day power system are more difficult to obtain than those of earlier. The numbers of very small distributed generation units and consumer self-generation from renewable, such as photovoltaic panels, are increasing and spread all over the system. Moreover, the demand side management (DSM) schemes, such as demand respond (DR), using price-based process are implemented in many consumer levels. As a result, in the high system load uncertainty is one of the most important issue in current power system.

Fortunately, the innovation in modern computer processor units has produced as a matter of engineering required to solve the complex problems in short time. Therefore, the probabilistic optimal power dispatch had been proposed in several research. The basic probabilistic load flow (PLF) solution [1] is based on linearizing the load flow functions around the expected value and using convolution to evaluate the relevant density functions of the output variables. The probabilristic optimal power flow (POPF) using parameter estimation by the percentile algorithm efficiently and effectively solves Weibull PDF parameters of the OPF variables was proposed in [2]. Similarly, PLF using Weibull PDFs of photovoltaic power generation is investigated in [3]. In order to describe the impact of uncertainties, such as fluctuation of bus loads and intermittent behavior of renewable generations, on the available load supply capability (ALSC) of distribution system accurately and comprehensively, [4] defines a series of meaningful indices for the probabilistic evaluation of ALSC, using Latin hypercube sampling-based Monte Carlo simulation (LHS-MCS). A validation of two proposed schemes of the point estimate method (PEM) is made, [5] not only for normal distributions but also different kinds of PDF, such as Weibull and generalized extreme value. A PEM based Nataf transformation to solve probabilistic multi-objective optimal power flow (MO-OPF) [6] problem considering fuel cost and emission as objectives. Uncertainties in the wind power output and load demand are considered.

In this paper, the probabilistic day-ahead optimal power dispatch (PDOPD) problem formulation, with price-based real-time demand respond (PRDR), is proposed. The Truncated normal probability distribution function (TNPDF) is used to represent the daily load uncertainties. The proposed method accentuates the probabilistic inquiries in PDOPD solutions. The empirical rule will perform with important TNPDF sampling method as a vital role in the computational procedure to avoid the infeasible LF results during the computation.

This paper was arranged into five Section, as follow. Section 2 introduces the model of uncertainties including DR schemes and probabilistic loading pattern. Section 3 represents the problem formulation of the PDOPD with PRDR programs, while the real power demand at load buses is represented by normal PDF with and without TNPDF model. Section 4 indicates the simulation results from the modified IEEE 30 buses test system. Then, Section 5 provides the conclusion.

2. DR Schemes and Probabilistic Load Pattern

There are basically two concept for DR programs [7-9] which are price-based programs (PBPs) and incentive-based programs (IBPs). PBPs are commonly interested for researchers who provoke the consumers voluntarily provide load reductions by reacting to economic gestures. In spite of IBPs the customers have bided the payments in order to report an exact amount of load reduction over a specified time interval. Many economists are convinced that they are the most direct and efficient DR programs suitable for competitive electricity markets and should be the focus of policymakers. The PRDR concept can be shown in Fig.1.

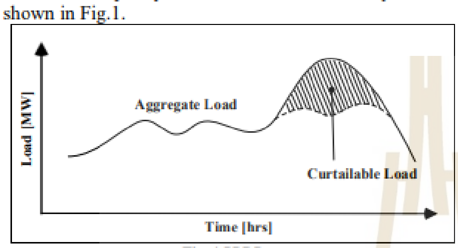

Fig. 1 PRDR concept

3. PDOPD Problem Formulation

3.1 PDOPD Problem Formulation

In this paper, the operating cost for each generator which is given by piecewise linear cost functions computed from the quadratic cost functions [10-11]. Therefore, the "hourly" objective function can be expressed by piecewise linear optimization model. The objective function can be expressed as,

$$\text{Minimize } TC = \sum_{i=1}^{NG}\sum_{j=1}^{NS_i} S_{ij}P_{G_{ij}} + \sum_{i=1}^{NB} D_i P_{DR_i}\ , \qquad (1)$$

subjected to the power balance constraint,

$$\sum_{i=1}^{NG} P_{G_i} + \sum_{i=1}^{NB} P_{DR_i} = \sum_{i=1}^{NB} \tilde{P}^o_{D_i} + P_{loss}\ , \qquad (2)$$

and the generator operating limit constraint,

$$P_{G_i}^{\min} \le P_{G_i} \le P_{G_i}^{\max}\ , i = 1,2,\ldots, NG, \qquad (3)$$

$$\sum_{i=1}^{NG} P_{G_i} = \sum_{i=1}^{NB} \tilde{P}_{D_i} + P_{loss}\ , \qquad (4)$$

$$\tilde{P}_{D_i} = \tilde{P}^o_{D_i} - P_{DR_i}\ , i = 1, 2, \ldots, NB, \qquad (5)$$

$$P_{Gi} = \sum_{j=1}^{NS_i} P_{G_{ij}} + P_{G_i}^{\min}\ , i = 1, 2, \ldots, NG, \qquad (6)$$

$$0 \le P_{G_{ij}} \le P_{G_{ij}}^{\max}\ , j = 1, 2, \ldots, NS_i, \qquad (7)$$

$$|f_{lm}| \le |f_{lm}|^{\max}\ , \qquad (8)$$

$$|V_i|^{\min} \le |V_i| \le |V_i|^{\max}\ , i = 1, 2, \ldots, NB. \qquad (9)$$

For the NRPF technique, the bus power injections including active and reactive power for every bus can be reproduced in polar coordinates and expressed as

$$P_{G_i} - \tilde{P}_{D_i} = \sum_{k=1}^{NB} |V_i||V_k||y_{ik}|\cos(\theta_{ik} - \delta_{ik}) \qquad (10)$$

$$Q_{G_i} - \tilde{Q}_{D_i} = -\sum_{k=1}^{NB} |V_i||V_k||y_{ik}|\sin(\theta_{ik} - \delta_{ik}) \qquad (11)$$

Where,

TC is the total system cost,
P_{Gi} is the real power generation at bus i,
S_{ij} is the linearized incremental cost curve for each segment of P_{Gi} at bus i,
D_i is the linearized incremental cost curve for each demand response at bus i,
NS_i is the number of segments of the linearized cost of the generator at bus i,
NG is the number of generators in the system,
NB is the number of buses in the system,
P_{DR_i} is the real power demand response at bus i,
$\tilde{P}_{D_i}$ is the probabilistic real power demand at bus i,
Q_{Gi} is the reactive power generation at bus i,
Q_{D_i} is the reactive power demand at bus i,
P_{loss} is the total transmission loss in the system,
$P_{G_i}^{\min}$ is the minimum real power generation at bus i,
$P_{G_i}^{\max}$ is the maximum real power generation at bus i,
$|f_{lm}|$ is the apparent power flow on the branch between bus l and m,
$|f_{lm}|^{\max}$ is the maximum limit at apparent power flow on the branch between bus l and m,
$|V_i|$ is the voltage magnitude at bus i,
$|V_i|^{\max}$ is the maximum voltage magnitude at bus i,
$|V_i|^{\min}$ is the minimum voltage magnitude at bus i,
$|y_{ik}|$ is the magnitude of the y_{ik} element of Y_{bus},
θ_{ik} is the angle of the y_{ik} element of Y_{bus}, and
δ_{ik} is the voltage angle difference between bus i and bus k.

The objective function in Eq.(1), with the constraints in Eqs. (2)-(9), is solved for 24 hours in order to obtain PDOPD solution, using Monte Carlo Simulation (MCS).

3.2 MCS for PDOPD

The MCS [12] is used for probabilistic power demand simulation and the PDOPD is run until the average total real power generation of the iteration $k+1$ (TPg_{avg}^{k+1}) is close to that of the iteration k (TPg_{avg}^{k}). More specifically, the MCS base OPD is run until $|TPg_{avg}^{k} - TPg_{avg}^{k+1}| < \varepsilon$, where ε is a very small real number. In this case study, the ε is set to 0.0001. The proposed framework of MCS procedure as,

Step 1: Read the initial system data for the required variables and offered price of generators and PRDR,

Step 2: Create the PDF of power demand at every specified bus i

Step 3: Execute the iteration k =1, where TPg_{avg}^{k} = 0,

Step 4: Determine the initial LF solution.

Step 5: Solving Eqs.(1) – (9) for optimal solution.

Step 6: Does the solution from **Step 5** matches the solution from **Step 4** ? If yes, go to **Step** 7, else, go to **Step 4**.

Step 7: whether $|TPg_{avg}^{k} - TPg_{avg}^{k+1}| < \varepsilon$? If yes, go to **Step 8**, or else, k = k+1 and go to **Step 4**.

Step 8: Compute total power generation and DR costs.

4. Results and Discussion

The one line diagram of the modified test system is shown in Fig. 2, besides, bus data, branch data, generator data, generators' operating costs, and other related data for this system following the standard IEEE 30-bus test system [13]. The proposed framework was performed by PDOPD computational procedure with simulation 2000 runs. The cases study are as follows;

- Base case with original LF solution
- Day-ahead Optimal power dispatch (OPD) without DR
- PDOPD using NPDF
- PDOPD using TNPDF case 1: $\mu \pm \sigma$
- PDOPD using TNPDF case 2: $\mu \pm 2\sigma$
- PDOPD using TNPDF case 3: $\mu \pm 3\sigma$

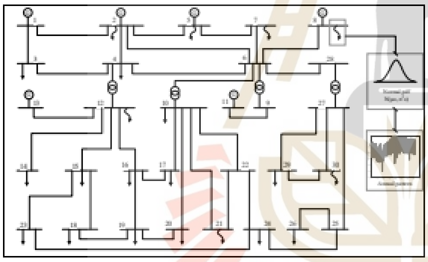

Fig. 2 Diagram of the Modified IEEE 30-bus Test System

Moreover, the pattern of the total system cost with and without DR program is shown in Fig.6 when the system loading represented by TNPDF sampling rules in order to confirm the practicality of the proposed setting. It is exposed that the proposed methods could offer the dispatch results and it provided the neglected error less than one percent because of the output data were provided with an average value during the simulations.

From the results, normal PDF sampling variables with the computational framework processed at least 1540 trials to meet the convergent solution. Involvement in this study, it was enhanced after applying the empirical rule mentioned in Section 3.8.3. They are complicated in the computational procedure by refining to give the convergent solutions at least 411 trials within one standard deviation (Case 1) and at least 817 trials within two standard deviations (Case 2). Otherwise, within three standard deviations (Case 3), the convergence has met at least 1406 trials parallel to the case of normal PDF sampling methods.

In Table 1, the POPD is run with normal PDF random variation input as loading uncertainties at the specified, which the size of P_{DR} was also enhanced from LP optimization to participate in the system and then it properly determined the total system operating cost dispatch 17,200 \$/day. In addition, the PRDR is still directed on the system planning for aggregate loads.

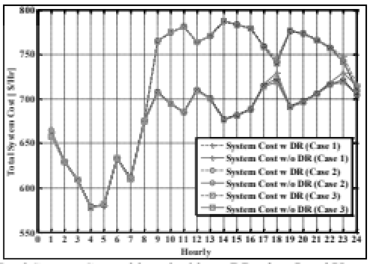

Fig. 6 Total System Cost with and without DR when Load Uncertainties represented by PTNF Sampling Methods

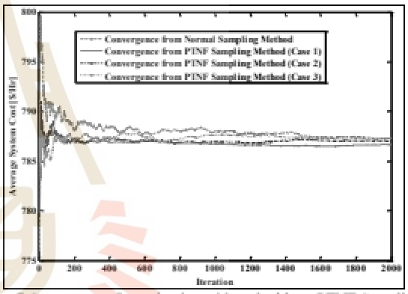

Fig. 7 Convergence Investigation with and without PTNF Sampling Methods

Table 1 Dispatch Results for Day-ahead

Variable	Base Case	DOPD w/o DR	PDOPD $N(\mu, \sigma)$	PDOPD with TNPDF *Case 1*	*Case 2*	*Case 3*
Total Generation [MWhr, MVARhr]	[7,885.6 ; 2002,7]	[7,885.2 ; 2,006.4]	[6,949 ; 1,980]	[6,950.8 ; 1,980.7]	[6,949.5 ; 1,980.9]	[6,949.3 ; 1,980.8]
Total P-Q Load [MWhr, MVARhr]	[7,806.2 ; 3,028.8]	[7,806 ; 3,028.8]	[6,876.5 ; 3,028.8]	[6,877.8 ; 3,028.8]	[6,876.2 ; 3,028.8]	[6,876 ; 3,028.8]
Total DR Size [MWhr]	–	–	[385.4]	[377.4]	[380.5]	[385]
Total Syst. Losses [MWhr, MVARhr]	[79.44 ; -412.32]	[78.96 ; -412.08]	[72.5 ; -438.77]	[73 ; -438.07]	[73.3 ; -437.81]	[73.3 ; -437.92]
Total Gen. Cost (\$/day)	18,996	17,739	16,178	16,228	16,206	16,181
Total DR Cost (\$/day)	–	–	1,022.6	1,001.6	1,009.7	1,022.6
Total Syst. Cost (\$/day)	18,996	17,739	17,200	17,229	17,216	17,204

The total cost for day-ahead resulted from the proposed method is shown to be the lowest among all cases. It had total system cost, of approximately 17,200 \$/day, less than those of the PEM solution [3]. Regarding the proposed method, the approximate system cost in both normal PDF and PTNF sampling methods is satisfactory to confirm the effectiveness of the proposed framework.

5. Conclusion

In this paper, the PDOPD, using TNPDF, considering PRDR problem formulation is proposed. The proposed PDOPD had been solved by LP and investigated by MCS. The predictable load uncertainties at the demand side are represented by the normal PDF with TNPDF sampling methods as input variations in the framework of the MCS procedure. The results shown that the proposed method can effectively and efficiently curtail the total power generation cost, while the PRDR is a trade-off between the total system operating cost and the PRDR providers. Meanwhile, the TNPDF sampling method can avoid infeasible solutions from the MCS, leading to the better convergence behavior in computation.

References

[1] Allan, R.N., Leite da Silva, A.M., and Burchett, R.C.. "Evaluation Methods and Accuracy in Probabilistic Load Flow Solutions," *IEEE Transactions on Power Apparatus and Systems*, 1981, PAS-100(5), pp. 2539-2546.

[2] Chayakulkheeree, K.. "Probabilistic Optimal Power Flow with Weibull Probability Distribution Function of System Loading using Percentiles Estimation," *Electric Power Components and Systems*, 2013, 41(3), pp. 252-270.

[3] Chayakulkheeree, K.. "Probabilistic Load Flow for High Penetration Solar Power Plant Distribution System using Percentile Estimation of Weibull Probability Distribution Function," *PEACON2015, Technology for Distribution System Development in the Future*, 2015, pp. 116-121.

[4] Zhang, S., Cheng, H., Zhang, L., Bazargan, M., and Yao, L.. "Probabilistic Evaluation of Available Load Supply Capability for Distribution System," *IEEE Transactions on Power Systems*, 2013, 28(3), pp. 3215-3225.

[5] Giraldo-Chavarriaga, J.S., Castrillón-Largo, J.A., and Granada-Echeverri, M.. "Stochastic AC Optimal Power Flow Considering the Probabilistic Behavior of the Wind, Loads and Line Parameters," *Ingeniería Investigación y Tecnología*, 2014, 15(4), pp. 529-538.

[6] Shargh, S., Khorshid ghazani, B., Mohammadi-ivatloo, B., Seyedi, H., and Abapour, M. "Probabilistic Multi-objective Optimal Power Flow Considering Correlated Wind Power and Load Uncertainties," *Renewable Energy*, 2016, vol. 94, pp. 10-21.

[7] Vardakas, J.S., Zorba, N., and Verikoukis, C.V., "A Survey on Demand Response Programs in Smart Grids: Pricing Methods and Optimization Algorithms," *IEEE Communication Surveys and Tutorials*, 17(1), 2015, pp.152-178.

[8] Paterakis, N.G., Erdinç, O., and Catalão, J.P.S., "An Overview of Demand Response: Key-elements and International Experience," *Renewable and Sustainable Energy Reviews*, 69, 2017, pp. 871-891.

[9] Chhor, U., Leeton, U., and Chayakulkheeree. "Probabilistic Optimal Power Dispatch Considering Price-based Real Time Demand Response," *International Journal of Intelligent Engineering and Systems*, 2019, vol. 12, no.1, pp. 201-210.

[10] Allen J. Wood, Bruce F. Wollenberg, and Gerald B. Sheblé, *Power Generation, Operation, and Control*, Third Edition, John Wiley & Sons, Inc, 2014.

[11] W. Ongsakul, S. Chirarattananon, and K. Chayakulkheeree, "Optimal Real Power Dispatching Algorithm for Auction Based Dispatch Problems," *Proceedings of International Conference on Power Systems (ICPS)*, CIGRE, China, 2001.

[12] M. H. Kalos and P. A. Whitlock, Monte Carlo Method, 2nd Edition, Wiley-VCH Verlag GmbH & Co. KGaA, Weinheim, 2008.

[13] Alsac, O. and Stott, B. "Optimal Load Flow with Steady-state Security," *IEEE Transactions on Power Apparatus Systems*, 1974, PAS-93(3), pp. 745-751.

Biography

Keerati Chayakulkheeree received his B. Eng. in EE from KMITL in 1995, M. Eng. and D. Eng. degree in Electric Power System Management from AIT, in 1999 and 2004, respectively. He is currently an associate professor at School of Electrical Engineering, Institute of Engineering, Suranaree University of Technology, Thailand.

Nithiwat Intharasomchai received his B. Eng. in EE from Suranaree University of Technology in 2019. He is currently a graduate student in power system program at Suranaree University of Technology (SUT). His current interests are in power system optimization algorithms and artificial intelligence.

Udoum Chhor received his B. Eng. degree in electrical and electronic engineering (EEE) from Institute of Technology of Cambodia (ITC), Cambodia in 2015, M. Eng. degree in power system program from Suranaree University of Technology in 2019. He is currently a lecturer of Department of Electrical Engineering, Faculty of Engineering, National Polytechnic Institute of Cambodia, Phnom Penh, Cambodia

2020 International Conference on Power, Energy and Innovations (ICPEI 2020)
October 14-16, 2020, Chiangmai, THAILAND

Steady State Primary Frequency Estimation for Microgrid Transferring Mode Using Distributed Slack Bus Load Flow Analysis

N. Intharasomchai and K. Chayakulkheeree
School of Electrical Engineering Institute of Engineering
Suranaree University of Technology
Nakhonratchasima, Thailand
keerati.ch@sut.ac.th

Abstract— This paper proposes a calculation method to determine the frequency deviation of microgrid (MG) system in transferring mode, using the mathematical model of distribution slack bus load flow (DSLF). In the proposed method, the modified incorporating Newton-Raphson load flow incorporating generation control equations are used to find the primary frequency deviation. The IEEE radian distribution 33-bus was modified as an microgrid model and used to test the proposed method.

Keywords*— Microgrid, Transferring mode of microgrid, frequency deviation and load flow*

Nomenclature

- F is actual system frequency,
- F_0 is schedule system frequency,
- NB is the number of buses,
- P_{G_i} is the real power generation at bus i,
- P_{D_i} is the real power demand at bus i,
- $P_{cal,i}$ is the real power flow calculate at bus i,
- Q_{G_i} is the reactive power generation at bus i,
- Q_{D_i} is the reactive power demand at bus i,
- $Q_{cal,i}$ is the reactive power flow calculate at bus i,
- P_{LOSS} is the total real power transmission loss in system,
- $P_{G_i^o}$ is the real power schedule at bus i,
- r_i is speed-droop setting on turbine governor in generating plant connected to bus i,
- $|V_i|$ is the voltage magnitude at bus i,
- $|Y_{i,k}|$ is the admittance magnitude of bus i and bus k,
- $\theta_{i,k}$ is the admittance angle of bus i and bus k,
- δ_i is the angle of voltage at bus i,
- α_i is the participation factor of generator connected to bus i,
- ΔF is steady-state frequency deviation,
- ΔG is static area control error,
- ΔP_{G_i} is the real power generation deviation at bus i,
- ΔP_i is the real power deviation at bus i,
- ΔQ_i is the reactive power deviation at bus i,
- $\mathbf{Y_{bus}}$ is the matrix of $Y_{k,i}$,
- $\mathbf{\Delta P}$ is the column matrix of ΔP_{G_i},
- $\mathbf{\Delta Q}$ is the column matrix of ΔQ_i,
- $\mathbf{\Delta\delta}$ is the column matrix of δ_i deviation,
- $\mathbf{\Delta|V|}$ is the column matrix of $|V_i|$ deviation.

I. Introduction

Therefore, with the high dramatically in distributed energy resources, many distribution systems have been shifted to MG structure. A MG is a local power grid with capability to disconnected from a main power grid (MPG). Moreover, MG can even supply the electricity to the MPG.

In common practice, the MG has two operating modes. However, which are grid connected and islanded modes unavailable when the MG is transferred in between these two modes of operation, the consequence is the frequency (primary control) and voltage deviation and the following consequence is the change of electric power generation (secondary control). The most of impact analysis for MG transferring mode are presented by simulation with the transfer function, which is difficult to analyze in a large system.

In the last decade, many researches related to the MG operation have been presented. Both the structure of the MG [1,2], which has been described as a microgrid is a cluster of distributed generations (DGs), energy storage, and loads within clearly defined electrical boundaries, which acts as a single controllable entity with respect to the grid, as defined by the MG Exchange Group, an ad hoc group of experts and implementers of MG technology. The operating condition of MG can be divided into different modes as shown in Fig 1.

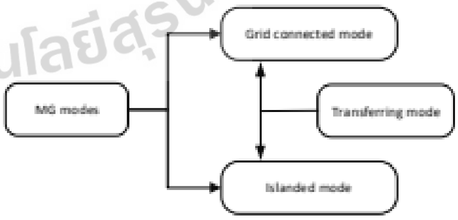

Fig. 1 Operation modes of MG.

There are also researches that discuss the effect of changing the MG mode [3-6]. However, most of the research simulated the MG system with the transfer function for analysis. Many research papers found that changing the MG operating mode affects the deviation of the primary frequency.

978-1-7281-7240-8/20/$31.00 ©2020 IEEE

2020 International Conference on Power, Energy and Innovations (ICPEI 2020)
October 14-16, 2020, Chiangmai, THAILAND

Therefore, being aware of the effects of changes in operating modes is very important. This paper purposes the concept of frequency analysis of the first control resulting from the effect of changing the MG mode by load flow simulation.

In the propose method, the mathematical model of distributed slack bus load flow (DSLF) program is used to find the exact frequency deviation, without the transfer function determination.

This paper was arranged into five Sections, as follows. Section II introduces equation of method involved in the frequency deviation analysis. Section III presents the models for simulating. Section IV indicates the simulation results from the modified 33 buses distribution system. Then, Section V provides the conclusion.

II. Steady State Frequency Deviation Analysis for MG

This section presents the method involved in the simulation to find the deviation of frequency in the MG primary control.

A. Distributed Slack Bus Load Flow (DSLF)

In this paper, the Newton-Raphson Power Flow (NRPF) technique [7-9] is used to incorporating generation frequency control characteristic. Bus power injections including active and reactive power for every bus and the Jacobian matrix can be expressed as,

$$\Delta P_i = (P_{G_i} - P_{D_i}) - P_{cal,i} \qquad i = 1, \ldots, NB, \tag{1}$$

$$\Delta Q_i = (Q_{G_i} - Q_{D_i}) - Q_{cal,i} \qquad i = 1, \ldots, NB, \tag{2}$$

$$P_{cal,i} = \sum_{k=1}^{NB} |V_i||V_k||Y_{i,k}|\cos\left(\theta_{i,k} + \delta_k - \delta_i\right), \ i = 1, \ldots, NB, \tag{3}$$

$$Q_{cal,i} = -\sum_{k=1}^{NB} |V_i||V_k||Y_{i,k}|\sin\left(\theta_{i,k} + \delta_k - \delta_i\right), \ i = 1, \ldots, NB, \tag{4}$$

$$\begin{bmatrix} \Delta \mathbf{P} \\ \Delta \mathbf{Q} \end{bmatrix} = \begin{bmatrix} \frac{\partial \mathbf{P}}{\partial \boldsymbol{\delta}} & \frac{\partial \mathbf{P}}{\partial |\mathbf{V}|} \\ \frac{\partial \mathbf{Q}}{\partial \boldsymbol{\delta}} & \frac{\partial \mathbf{Q}}{\partial |\mathbf{V}|} \end{bmatrix} \begin{bmatrix} \Delta \boldsymbol{\delta} \\ \Delta |\mathbf{V}| \end{bmatrix}, \tag{5}$$

and generator's prime mover responses and AGC action [10] are included as primary and secondary controls. Active power generation at a bus considered as,

$$\sum_{i=1}^{NG} P_{G_i} = \sum_{i=1}^{NG} P_{G_i^o} + \sum_{i=1}^{NG} \Delta P_{G_i}, \ i = 1, \ldots, NB, \tag{6}$$

$$\Delta P_{G_i} = -\frac{1}{r_i}\Delta F + \alpha_i \Delta G, \ i = 1, \ldots, NB, \tag{7}$$

$$\sum_{i=1}^{NG} \alpha_i = 1.00, \ i = 1, \ldots, NB, \tag{8}$$

$$\Delta F = F - F_0 \,. \tag{9}$$

B. DSLF for MG Frequency Deviation Analysis

Assuming bus one as reference for the purpose of frequency deviation calculations of the system, the linearized equations for Newton-Raphson is corrected from Eq. (5) can be expressed as,

$$\begin{bmatrix} \Delta P_1 \\ \Delta \mathbf{P}_{2\text{-}NB} \\ \Delta \mathbf{Q} \end{bmatrix} = \begin{bmatrix} \frac{\partial \mathbf{P}}{\partial \mathbf{F}} & \frac{\partial \mathbf{P}}{\partial \boldsymbol{\delta}_{2\text{-}NB}} & \frac{\partial \mathbf{P}}{\partial |\mathbf{V}|} \\ \frac{\partial \mathbf{Q}}{\partial \boldsymbol{\delta}_1} & \frac{\partial \mathbf{Q}}{\partial \boldsymbol{\delta}_{2\text{-}NB}} & \frac{\partial \mathbf{Q}}{\partial |\mathbf{V}|} \end{bmatrix} \begin{bmatrix} \Delta F \\ \Delta \boldsymbol{\delta} \\ \Delta |\mathbf{V}| \end{bmatrix}. \tag{10}$$

Therefore, this concept can be find the ΔF in primary responsewhen there is sudden change of generation or load so, that is also a simpler and more convenient method than using transfer function.

The iterative process is repeated until ΔP_i in Eq. (10) and ΔQ_i in Eq. (5) for all buses are within a specified tolerance. The computational procedure is shown in Fig. 2.

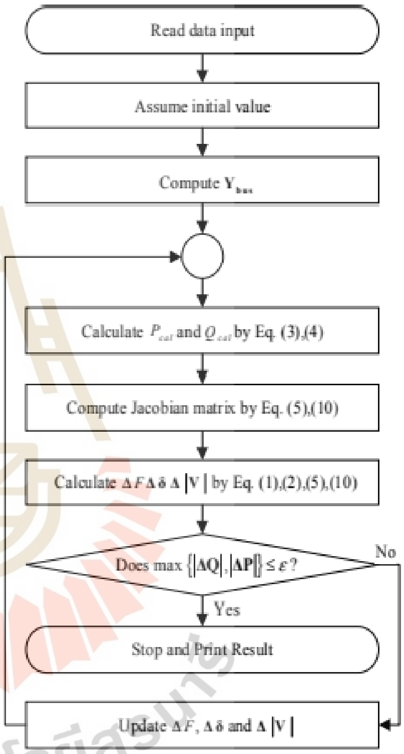

Fig. 2 Computational procedure of power flow program for finding of the frequency deviation.

III. MG Transferring Mode Model

The test system model was modified from IEEE radian distribution 33-bus [11-13] by placing the generators at bus 13, 22 and 28, while bus 1 is connected to the MPG as show in Figure 3. The generation placement in the test system is resulted from total power loss and generation cost minimization [13].

2020 International Conference on Power, Energy and Innovations (ICPEI 2020)
October 14-16, 2020, Chiangmai, THAILAND

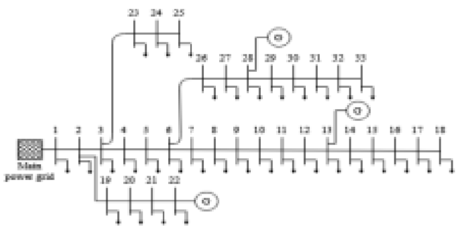

Fig. 3 Modified IEEE radian distribution system 33-bus

The proposed framework in section II was performed by DSLF computational procedure with simulation to find frequency deviation in systems with these case study as follow;

- Case 1: The load is distributed from the grid system to the microgrid, so that bus one is like a generator bus.
- Case 2: The load is distributed from the microgrid to the grid system, so that bus one is like a load bus.

Therefore, disconnecting while the MG is under case 1 is the same concept generation outage and under case 2 it is load outage behavior as shown in Fig. 4.

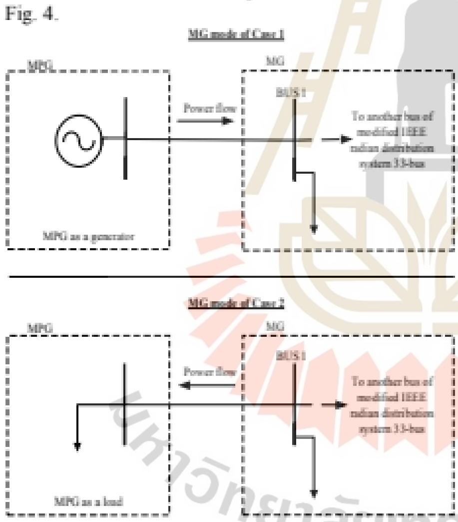

Fig. 4 Assume main grid for case study

IV. Simulation Result

This section presents the results of Case 1 and 2. Which the simulation references of the modified IEEE radian distribution system 33-bus, in Fig 3.

The comparison on grid connected status, primary control after and transfer, secondary control after transfer is addressed for both cases.

A. Simulation Result of Case 1

In the simulation of Case 1, while the MPG supplies power to MG 235.4 kW before MG is connected. The total power generation including power supply from MPG is 3,715 kW before MG is disconnected and changing the status of MG to islanded mode. The impact on system control both primary and secondary controls is shown in Table 1.

Table 1 Simulation Results of Case 1

Power flow (kW)	Before transfer	After transfer	
		Primary control	Secondary control
MPG	235.4	0	0
P_{G13}	804.3	804.3	816.9
P_{G22}	1,557.6	1,557.6	1,581.9
P_{G28}	1,326.1	1,326.1	1,346.8
Power Generation	3,923.4	3,688.0	3,745.6
Power Demand	3,715.0	3,715.0	3,715.0
Power Loss	208.4	-	30.55
Frequency (Hz)	50	49.882	50

Based on the results of the experiment in Table 1, the primary control power generation does not change, but the frequency falls because the primary control adjusts the frequency to control the power as in Eq. (7). On the other hand, the secondary control frequency is controlled to 50 Hz as it should, but the power generation is revalued to respond according to the load. All generators are adjusted to compensate for the power generation that is lost from the main power grid. The total power generation without power supply from MPG is 3,745.6 kW, after secondary control action. The simulation result for steady state frequency deviation can be illustrated in Fig. 5. Note that the power loss is reduced from 208.4 kW to 30.55 kW, due to increasing in local generation, leading to the lower total power generation after transferring of MG mode.

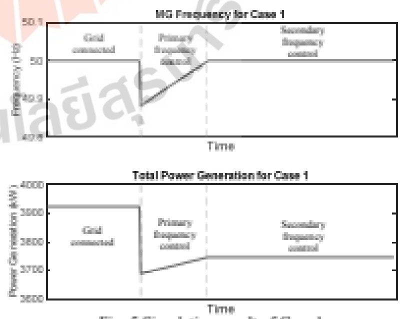

Fig. 5 Simulation result of Case 1

B. Simulation Result of Case 2

In Case 2, the main power grid receives power from the MG 185.75 kW, in connected mode, before MG is disconnected, changing the status of MG to change to islanded mode. The effect of disconnection

2020 International Conference on Power, Energy and Innovations (ICPEI 2020)
October 14-16, 2020, Chiangmai, THAILAND

on system control both primary and secondary controls are shown in Table 2.

Table 2 Simulation Result of Case 2

Power flow (kW)	**Before transfer**	**After transfer**	
		Primary control	**Secondary control**
main power grid	-185.75	0	0
P_{G13}	858.8	858.8	816.9
P_{G22}	1,663.1	1,663.1	1,581.9
P_{G28}	1,415.9	1,415.9	1,346.8
Power Generation	3,937.8	3,937.8	3,745.6
Power Demand	3,900.75	3,715.0	3,715.0
Power Loss	37.75	-	30.55
Frequency (Hz)	50	50.393	50

From the experimental results in Table 1, power generation of primary control has not changed. But the frequency increases to 50.393 Hz, because the primary control will adjust the frequency to control the power, as in Eq. (7). On the contrary, the power generation of the secondary control is stable at 50 Hz. From the experimental Table 2, the secondary control power generation has decreased due to the decrease in the load at the main power grid, resulting in a reduce power generation. The simulation result for steady state frequency deviation can be illustrated in Fig. 6.

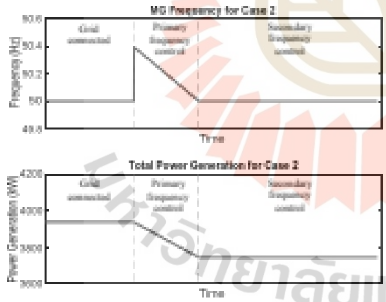

Fig. 6 Simulation result of Case 2

V. Conclution

Frequency deviation is an important factor in controlling MG's operation. Therefore, it is necessary to study several methods of MG frequency deviation analysis. In this paper, DSLF is introduced to determine the steady-state frequency of MG transferring mode. The proposed method can be used for pre-determining the frequency deviation in the MG operation, using steady state load flow model.

References

[1] Y. R. Kukandeh and M. H. Kazemi, "Microgrid Control in Islanding and Connected Mode," ICEE., 2018, DOI. 10.1109/ICEE.2018.8472560.

[2] Q. Fu, A. Nasiri, A. Solanki, A. B. Ahmed, L. Weber, and V. Bhavaraju, "Microgrids: Architectures, Controls, Protection, and Demonstration," Electric Power Components and Systems, vol.43, no.12, pp.1453–1465, 2015.

[3] M. Prakash.M and J. Paul, "Control of Microgrid for Different Modes of Operation," International Journal of Engineering Research & Technology, vol. 5, no. 05, pp. 815-820, 2016.

[4] J. H. Zheng, Y. T. Wang, Z. J. Wang, S. Zhu, X. Wang and S. Xinwei, "Study on microgrid operation modes switching based on eigenvalue analysis," International Conference on Advanced Power System Automation and Protection, 2011, DOI. 10.1109/APAP.2011.6180443.

[5] S. Mansour, M. I. Marei and A. A. Sattar, "Droop based Control Strategy for a Microgrid," Global Journal of Researches in Engineering: F Electrical and Electronics Engineering, vol. 16, no. 7, 2016.

[6] L. I. U. Meiyin, L. V. Zhenhua, W. U. Beibei , G. U. O. Chongyang, and H.A.N. Pingping, "Research on Switching Model of Microgrid with Distributed Power Supply," ICSREE, 2018, DOI. 10.1051/e3sconf/20185703008

[7] T. Wu, Z. Alaywan, and A. D. Papalexopoulos, "Locational Marginal Price Calculations Using the Distributed-Slack Power-Flow Formulation," IEEE TRANSACTIONS ON POWER SYSTEMS, vol. 20, no. 2, pp. 1188-1190, 2005.

[8] P. Yan, "Modified Distributed Slack Bus Load Flow Algorithm for Determining Economic Dispatch in Deregulated Power Systems," PESW, pp. 1226-1231, 2001.

[9] K. Chayakulkheeree, "Application of distributed slack bus power flow to competitive environments," AUPEC, paper no.20-16, pp. 531–536, 2007.

[10] A. J. Wood, B. F. Wollengerg, G. B. Sheblé (Eds.), 2014 "Power Generation, Operation, And control," vol. 3rd, Canada, John Wiley & Sons.

[11] P. Díaz, M. P. Cisneros, E. Cuevas, O. Camarena, F. Fausto and A. González, "A Swarm Approach for Improving Voltage Profiles and Reduce Power Loss on Electrical Distribution Networks," IEEE Access, vol. 6, pp. 49498-49512, 2018.

[12] V. Vita, "Development of a Decision-Making Algorithm for the Optimum Size and Placement of Distributed Generation Units in Distribution Networks," Energies, vol. 10, pp. 1433-1446, 2017.

[13] M. Mousavi, A. M. Ranjbar, A. Safdarian, "Optimal DG Placement and Sizing Based on MICP in Radial Distribution Networks," Smart Grid Conference (SGC), 2017,

BIOGRAPHY

Nithiwat Intharasomchai was born on April 18, 1997 in Nakhonratchasima Province, Thailand. He received his Bachelor's Degree in Engineering (Electrical Engineering) from Suranaree University of Technology in 2019. He continued with his graduate studies in the Electrical Engineering at Suranaree University of Technology. His current interests are in power system optimization algorithms and artificial intelligence.